APPENDIX A

PLASMA IN THE MAGNETOSPHERE

06500-6004-R000

15 December 1966

PLASMA IN THE MAGNETOSPHERE

by

Frederick L. Scarf

Prepared for

Volume I of Advances in Plasma Physics

edited by

W. Thompson and A. Simon

Interscience Press

SPACE SCIENCES LABORATORY
SYSTEMS LABORATORIES

TRW SYSTEMS
One Space Park
Redondo Beach, California 90278

PLASMA IN THE MAGNETOSPHERE*

Frederick L. Scarf

Space Sciences Laboratory
TRW Systems
Redondo Beach, California

1. INTRODUCTION

The earth and its magnetic field form an obstacle in the path of the continuously streaming collisionless plasma which represents the outer corona of the sun, and this solar wind compresses and distorts the geomagnetic dipole field into a cavity which is referred to as the magnetosphere. The average boundary of this cavity is located at about 10 earth radii in the solar direction, and the cross-sectional diameter is on the order of 50-70 R_e on the night side. The distorted geomagnetic field appears to extend over a huge tail region in the anti-solar direction, and present estimates of the tail length are on the order of one-thousand earth radii, or more. The magnetosphere contains a very complex distribution of charged particles and it represents a valuable plasma laboratory in which wave propagation, containment, injection, local particle acceleration, plasma instabilities, and other non-linear phenomena can be studied without many of the difficulties and degrading effects encountered in the ground-based laboratory.

Prepared for Volume I of Advances in Plasma Physics, edited by W. Thompson and A. Simon, Interscience Press.

In this review, we present a summary of some of the more important characteristics of this magnetosphere, and call attention to those areas which appear to be of greatest interest for plasma physics investigations. The summary is necessarily severely limited because space physics, and especially spacecraft physics, is a very young science. Most of the phenomena to be discussed can only be studied experimentally by examining the response of a small number of instruments on a satellite, and no scientific satellites were available, even in low earth orbits, until 1957 and 1958. Moreover, a single spacecraft travels on an isolated trajectory in space-time, and many successive passes are needed in order to map spatial characteristics during a given time interval; however, Explorer 12, the first long-lived earth orbiter to penetrate the boundary of the magnetosphere, was not launched until March 25, 1961. Similarly, no extensive mapping of the near-earth magnetospheric tail was possible until Explorer 18 (IMP-1) was launched toward the end of 1963. Thus, we are only beginning to obtain complete spatial coverage of the magnetosphere, and although the characteristics discussed below are consistent with the results of present measurements, the field is certainly not closed.

A second problem which must be faced when an attempt is made to evaluate the available body of knowledge concerns the effect of temporal variations. The orientation, size, shape, and content of the magnetosphere are all strongly influenced by the state of the interplanetary plasma stream and its imbedded magnetic field. At any point in the magnetosphere it is probable that diurnal variations, 27-day variations (corresponding to the solar rotation period as enhanced corotating interplanetary features sweep across the earth), eleven-year variations (corresponding to the secular

cycle of solar activity), etc. will all be discernible, as well as transient effects associated with isolated solar storms, flares, etc. Since the exploration of the outer magnetosphere is now only a few years old, it is clear that study of the temporal variations is necessarily incomplete.

Aside from these difficulties associated with the huge volume of the magnetosphere, the restrictions of orbital mechanics, and the variable nature of the sources of magnetospheric phenomena, spacecraft physics presents some additional unique problems. Spacecraft weight, power, and telemetry are severely limited, and related measurements must generally be made in a sequential pattern. Unknown or uncontrollable biases may be present and sources of contamination involving spacecraft magnetic fields, the plasma sheath surrounding the vehicle, external electromagnetic or electrostatic interference, photoelectron currents, etc. have degraded many experimental programs. Another problem area stems from the requirement of a huge dynamic range to characterize particle and field distributions in the magnetosphere. In most cases adequate range or sensitivity switching is impossible, and many discoveries of sharp "boundaries" have turned out to be associated with threshold response for the instrument in question; other detectors have yielded completely different information, and any assessment of magnetospheric experiments must involve consideration of the types of sensors involved.

For all of these reasons, it should be appreciated that the study of plasma in the magnetosphere is a new field in which few generalizations can now be stated with a great deal of certainty. However, it should

also be apparent that many exciting discoveries remain to be made in this natural plasma laboratory which can be continuously probed on a microscopic scale, with production of relatively little disturbance by the orbiting measuring platform.

The discussion below explores selected topics in space physics, and no special effort is made to present the correct historical basis for the material, give appropriate credit for early discoveries, or include a comprehensive list of references. Those papers which have proven to be of most use to the author are cited, and these can be used to obtain more complete information.

2. THE STRUCTURE OF THE MAGNETOSPHERE

The idea that the geomagnetic field might be compressed into a finite volume by a stream of plasma from the sun was originally suggested by Chapman and Ferraro[1] in order to explain geomagnetic storm effects observed on the earth's surface. It was proposed that intermittent collisionless solar plasma flow might temporarily compress the dipole-like main field, and extensive calculations of the size and shape of the cavity were carried out. Parker's[2] prediction that the solar corona was in a continuous state of motion, arriving at the earth with a streaming speed on the order of several hundred kilometers/sec, contained the implicit suggestion that the Chapman-Ferraro cavity should be a permanent, rather than transient, feature of the solar wind-geomagnetic field interaction. The presence of a continuous solar wind, and the permanent existence of this cavity, called the magnetosphere, have now been fully confirmed, and a complete account of the theories of solar plasma flow, the early interplanetary measurements, and some terrestrial consequences of this flow is contained in the Jet Propulsion Laboratory Conference Report, "The Solar Wind"[3].

The most basic features of the solar wind-geomagnetic field interaction can be illustrated with a familiar magnetohydrodynamic model. For a non-viscous, highly-conducting plasma, the mhd momentum equation is

$$\rho \frac{\partial \vec{u}}{\partial t} + \rho(\vec{u}\cdot\vec{\nabla})\vec{u} + \vec{\nabla}P = -\frac{\vec{\nabla}B^2}{8\pi} + \frac{(\vec{B}\cdot\vec{\nabla})\vec{B}}{4\pi} \qquad (1)$$

where $\rho = N_e m + N_i M$ and $P = N_e \kappa T_e + N_i \kappa T_i$. If $\vec{B} = B(x)\vec{i}_z$, $\vec{u} = u(x)\vec{i}_x$, $P = P(x)$, then Eq. (1) and the continuity equation lead to the steady state relation

$$\rho u^2 + P + \frac{B^2}{8\pi} = \text{constant.} \tag{2}$$

Consider now the interaction which occurs when a uniform, unmagnetized plasma stream with asymptotic flow parameters ρ_o, u_o, P_o is incident along the negative x-axis toward a plasma-free region with an externally imposed magnetic field, $B(x) = B_o(x)$. If we assume that in a sheath with $x = x_b \pm \delta/2$, surface currents freely arise to shield out the $B_o(x)$ field, then

$$[\rho u^2 + P]_{x_b + \delta/2} = \left[\frac{B_T^2(x)}{8\pi}\right]_{x_b - \delta/2}, \tag{3}$$

where B_T, the total field, is $(B_o + B_s)$, and B_s is the field associated with the surface currents. However, B_T is to vanish just beyond $(x_b + \delta/2)$, and the current sheath centered at x_b must produce a field equal to $-B_o(x)$ in this upstream region. Since the induced field changes sign across the current sheath, $B_T(x_b - \delta/2)$ must equal $2B_o(x_b)$ for small δ. Finally, the particle density at x_b is twice the incident density because the hypothetical sheath turns all particles around, and thus the Chapman-Ferraro pressure balance relation is

$$2\,(\rho_o u_o^2 + P_o) \simeq \frac{[2B_o(x_b)]^2}{8\pi}. \tag{4}$$

Equation (4) easily leads to a reasonable estimate of the distance to the magnetosphere boundary, or magnetopause at the subsolar point (i.e., in the direction of the sun). The geomagnetic field without the surface current has a dipole component,

$$\vec{B}_D = -B_D^{(o)} \left(\frac{R_e}{r}\right)^3 (\vec{i}_\theta \sin\theta_m + 2\vec{i}_r \cos\theta_m) \qquad (5)$$

with $B_D^{(o)} = 0.312$ gauss, $R_e \simeq 6371$ km, and θ_m = geomagnetic colatitude; there are also contributions from higher order moments, ionosphere currents, ring currents, the tail current (see below) and other diamagnetic effects. However, at great distances ($r \gtrsim 7\ R_e$), Eq. (5) adequately represents the geomagnetic field in the region near local noon (i.e., solar ecliptic longitude, ϕ, near zero degrees) with $\theta_m \simeq \pi/2$. Just within the magnetosphere boundary, the surface currents must then yield a total field magnitude $B_T(r_b) = 2B_D(r_b) = 2B_D^{(o)}(R_e/r_b)^3$, and the most recent solar wind measurements indicate that $u_o \simeq 380$ km/sec, $N_o \simeq 5$ electron-proton pairs/cm^3, with $P_o << \rho_o u_o^2$ [4]. All of these numbers are consistent with Eq. (4) if the subsolar magnetopause is located at $r_b \simeq 9.3\ R_e$. This rather crude estimate is actually in fairly good agreement with spacecraft observations. For instance, on the first few inbound passes of IMP-1 (Explorer 18) with $\theta_m \simeq -8.3°$ to $-9.5°$, $\phi < 15°$, the streaming proton flux dropped below threshold for the Ames Research Center electrostatic analyzer at $r \simeq (10.3\text{-}11.1)\ R_e$ [4].

More elaborate investigations which include the three-dimensional nature of the problem and the fact that the solar wind does not flow all the way to the magnetopause in a smooth manner must be undertaken in order to

extend these calculations to obtain the true structure of the magnetosphere. For instance, although single particle coulomb collisions are unimportant in the solar wind, individual particles may be scattered by organized groups of particles, or waves, and the flow is not Newtonian, as we have assumed in deriving Eq. (4). The solar wind carries with it an imbedded extension of the photospheric field and near the earth $B_I \simeq 5 \times 10^{-5}$ gauss = 5 gamma. This magnetized collisionless plasma admits a great variety of wave motions and the modes with the longest wavelengths, which might be strongly generated by the huge obstacle which the magnetosphere presents to the solar wind, have group and phase velocities on the order of the Alfvén speed, $B_I/(4\pi N_o M_i)^{1/2} \simeq$ 50-80 km/sec. Thus, the solar wind flow is highly "supersonic" with respect to long wavelength transverse modes, and this fact was used to predict that the magnetosphere should create a "bow shock", with the standoff distance given roughly by fluid analogies based on the Alfvén or magnetosonic Mach numbers[5].

The basic mechanisms and the details of the fluid-like shock transition in a collisionless plasma are not well understood, but the fluid analogies can be used to show that the Chapman-Ferraro predictions do yield approximately the correct size and shape on the day side. In the transition region (i.e., between the shock and the magnetopause) N' and T' exceed N_o, T_o and u' is smaller than u_o, however Lees has shown[6] that the total mechanical pressure on the geomagnetic field is very nearly the same as the interplanetary value. At the stagnation point $u' \to 0$ but $P' \simeq 5(2\rho_o u_o^2)/12$ so that $r_b' \simeq 1.16\, r_b$ where r_b is the Newtonian value described above and r_b' takes into account a shock transition.

The three-dimensional generalization of Eq. (4) is mathematically complex, and some new theoretical uncertainties energe when this problem is studied. If it is assumed that all currents flow on the surface of a well-defined cavity then the Chapman-Ferraro problem may be generalized in a unique manner. Mead, Beard, and Midgely [7,8,9] have obtained approximate solutions to this problem, and within the magnetosphere an approximate representation for the surface current field is

$$B_X = 0.21\ (R_e/r_b)^4\ (Z/R_e)\ \text{gauss}$$
$$B_Y = 0$$
$$B_Z = [0.43 + 0.21\ (R_e/r_b)^4\ (X/R_e)]\ \text{gauss} \qquad (6)$$

in a cartesian system with the plus x-axis pointed toward the sun, and the z-axis toward the North Star (we neglect the 23° inclination of the earth's rotational axis to the ecliptic and the distinction between the geomagnetic and geographic poles).

The total field line configuration in the noon-midnight meridian plane is shown in Fig. 1a, along with the undistorted geomagnetic dipole. With $r_b \sim 10\ R_e$, the critical latitude separating field lines crossing the equator along the noon meridian from those crossing along the midnight meridian is about 83°. In Fig. 1b, the Chapman-Ferraro surface current consistent with Fig. 1a is schematically illustrated by the solid curves.

A second current system is illustrated by the dotted lines in Fig. 1b. Piddington[10] first suggested that some dissipation mechanism associated with the complex interaction between the solar wind and the

geomagnetic field might "stretch" the tail by causing the surface currents to flow across the top and bottom of the magnetosphere as shown; the hypothetical return currents would then flow toward the opposite direction in the interior plane containing the anti-solar direction. Hence current systems would encircle each half of the night-side cavity, producing a nearly neutral sheet in the tail. In Fig. 2 an attempt is made to illustrate the three dimensional configuration of the bow shock, the magnetosphere with a tail field, and the current system which produces this structure.

The existence of a tail field was anticipated and widely discussed on rather general grounds, and at present there is little theoretical basis for any quantitative discussion of the magnitude of the tail currents, etc., since the fundamental interaction which produces the geomagnetic tail has not been identified unambiguously. However, some speculations concerning the properties of the tail seem to have merit.

By analyzing regular magnetic field variations on the earth's surface it has been possible to establish that various current systems exist in the lower magnetosphere and ionosphere. One of these, the DS current system, is apparently associated with an electric field across the magnetosphere with positive potential on the morning side and negative on the evening side. The DS pattern is a high latitude phenomenon, and the driving electric field is thought to be related to the drift motion of interplanetary field lines past the magnetosphere and the formation of the geomagnetic tail. In one model[11, 12] an interplanetary field line

becomes "attached" to the geomagnetic field in the region of local noon and $\theta_M \simeq 75°$. The terrestrial end of this line then moves across the pole with speed $|\vec{E}_{TAIL} \times \vec{B}_{GEOMAG}| \simeq$ hundreds of meters/second and it becomes "detached" when $\theta_M \simeq 67°$, near midnight (determined by analyzing the DS pattern). During this time, the interplanetary medium has moved behind the earth with a typical solar wind speed of hundreds of kilometers/sec. It has therefore been proposed that the tail length is roughly the distance traveled by the solar plasma in the time during which an individual interplanetary field line is attached to the earth. This reasoning predicts that the geomagnetic tail length is on the order of 10^3 earth radii.

Related considerations yield an estimate of the distant tail cross-section. If we assume that the field lines which leave the earth within 20° of the poles stream out to form the tail, then conservation of flux suggests that the tail must expand to a radius of (25-35) R_e before the field magnitude drops to a typical interplanetary value of 5 γ.[13]

Although the presently available observations cover only very restricted portions of the magnetosphere, satellite measurements do tend to support the above discussion to a large extent. The magnetospheric cavity described by Eqs. 5, 6 has a nominal equatorial termination near 10 R_e at noon ($\phi \simeq 0°$) and just past 13 R_e at dusk ($\phi \simeq 90°$), with $(B_{TOTAL} - B_{GEOMAG}) \simeq$ (20-30) γ in the entire sunlit portion of the outer magnetosphere. Fig. 3 shows the magnetic measurements made as Pioneer 6 traversed the outer magnetosphere and magnetopause, and the curve labeled "theoretical" is actually the extrapolated dipole field magnitude[14]. It can be seen that the total field rose until $\overline{F} = |\vec{B}_T|$ approached 2 B_G at

the magnetopause, and just beyond this current sheath the typically noisy transition region fields were encountered (significant rms deviations presented on the bottom indicate the presence of high frequency oscillations). The magnetopause location agrees well with the predictions of Eqs. 5, 6.

Figure 4 shows magnetic measurements made by Ness, et al.[15] on IMP-1 in the tail region (Orbit 41, May 2-4, 1964) and it is clear that the field orientation becomes anti-solar ($\phi \sim 180°$) at large distances ($r > 16\ R_e$, spacecraft below the ecliptic). At 16 R_e, the field magnitude dips, and the field direction changes abruptly. This is representative of the traversal of the "neutral" sheet or surface in the earth's tail, but the field does not actually vanish. As reported by Speiser and Ness,[16] some finite connection of northern and southern hemispheric field lines across the geomagnetic tail was present during the active lifetime of IMP-1, and it was impossible to state unambiguously whether or not a truly neutral sheet existed. A sketch of the extended field lines in the tail for a period when the earth's magnetic axis had a significant tilt with the respect to the ecliptic (χ_{SS}, the magnetic latitude of the sub-solar point $\simeq 25°$) is shown in Fig. 5. From measurements such as these, Speiser and Ness were able to evaluate $(\vec{\nabla} \times \vec{B})$ to obtain $|\vec{J}|$, the neutral sheet return current density (see Fig. 2) which produces the tail field. Typical J values for $15\ R_e < r < 30\ R_e$ in the anti-solar direction were on the order of $3 - 5 \times 10^{-2}$ amp/m^2 with an accuracy of $\pm$ 10-20%.

Some direct information about the extent of the geomagnetic tail has recently become available. Soft solar flare electrons ($E > 30$-40 keV) were observed on IMP-3 when the spacecraft was well within the tail, but the temporal variation of the intensity and the delay time with respect to the solar disturbance did not differ significantly from the values obtained for similar interplanetary events. Lin and Anderson[17] argued that these electrons must have entered the tail at a distant point where at least some of the geomagnetic field lines connect directly into interplanetary field lines behind the earth, and they demonstrated that this point must have been no more than 5000 R_e downstream. Finally, the plasma probes on the Pioneer 7 spacecraft directly detected a solar wind cutoff as the tail was encountered 850 R_e behind the earth (J. Wolfe, private communication).

3. THERMAL PLASMA IN THE MAGNETOSPHERE

Most of our information about the distribution of thermal plasma in the magnetosphere comes from ground-based study of discrete electromagnetic waves called whistlers. Storey[18] first suggested that natural whistlers are noise signals, generated by lightning flashes, which travel out into the magnetosphere along geomagnetic field lines in the right hand polarization mode, $n^2 = R$. For $\vec{k} \times \vec{B} = 0$, the index of refraction in the zero temperature approximation is[19]

$$n^2 = 1 - \frac{\Omega_p^2}{\omega(\omega+\Omega_c)} - \frac{\omega_p^2}{\omega(\omega-\omega_c)} \quad , \tag{7}$$

where Ω_p, $\omega_p = (4\pi Ne^2/M,m)^{1/2}$ are the ion and electron plasma frequencies and Ω_e, $\omega_c = eB/(M,m)c$ are the ion and electron gyrofrequencies. In the frequency range $\Omega_c << \omega < \omega_c/2$, the group velocity of any component is found to be approximately

$$V_g(\omega) \simeq 2c\left[\frac{\omega\omega_c}{\omega_p^2}\left(1 - \frac{\omega}{\omega_c}\right)^3\right]^{1/2} \tag{8}$$

and a broad-band signal injected into the magnetosphere is widely dispersed as it travels along the field line out to the equator, and back to the earth in the opposite hemisphere. The original lightning noise impulse has all frequencies produced at a given time but the incoming signal arrives after a single hop along a field line with a distinctive frequency versus time variation because individual components have different travel times. The lowest frequency signals are the last to arrive

($V_g(\omega) \propto \omega^{1/2}$ for $\omega << \omega_c$) and the frequency range is generally in the audio band since f must be less than the equatorial gyrofrequency, $\omega_c\ (r_{max})/2\pi \simeq 880\ (R_e/r_{max})^3$ kc/s; these characteristics give rise to the name "whistler".

Detailed inspection of whistler traces reveals that the noise signals which traverse the magnetosphere and come down to the surface do follow the geomagnetic field lines very closely. Although the basic reason for this phenomenon is still not completely understood (ducting by field-aligned density gradients and stimulation of growing field-aligned waves have been proposed; this is discussed further below), it is an established fact that Eq. (7) holds over the curving field line and one can use the continuum of frequency versus time values in the received signal to determine the trajectory unambiguously. In parts (a), (b) of Fig. 6 some typical whistler paths and (f-t) diagrams are depicted, and Fig. 7 shows some actual whistler spectrograms. The total magnetospheric travel time at any one frequency can also be measured, either by locating the undispersed "spheric" which represents sub-ionospheric reception of the original lightning impulse, or by examining the time delays for successive echoes. The travel time yields the integrated electron density along the path.

In the last few years, huge numbers of whistler traces have been analyzed in an attempt to evaluate $N_e(\vec{r}, t)$. A given functional form for the density distribution along a field line is assumed and used to compute the equatorial density by determining the path and the time delay for a given whistler signal. The self-consistency of the assumed profile is then tested by making a distribution of all of the $N_e\ (\theta_M = \pi/2, r = r_{max})$

points obtained from the entire collection of whistlers. The density distributions which do not meet the test of self-consistency are discarded, and the process is then repeated using an improved form of $N_e(r, \theta_M)$, etc.

The initial results of this program were perplexing. Density distributions such as $N_e \simeq 10^4 \, (R_e/r)^3 \text{ cm}^{-3}$ appeared to be self-consistent in the sense described above[20], however there seemed to be no theoretical way to understand this result. Specifically, if we compute the mean free path, ℓ, along a field line with $N_e \geq 10^2 \text{ cm}^3$ ($r < 5 \, R_e$) and take $T_e \sim 2000°K$, we find that ℓ is never longer than about $0.5 \, R_e$. Thus, the mean free path is quite small compared to the length of the field line, and a collisional diffusive equilibrium distribution, with much more moderate density gradients should prevail.

The resolution of this problem required clear identification and separation of temporal and spatial variations in the plasma distribution. Carpenter[21] showed that attempts to construct an instantaneous electron profile by analyzing a whistler train, covering many different magnetospheric paths simultaneously, frequently required the use of two distinct forms for $N_e(r)$ to account for the measured time delays. In particular, the times for longer paths were found to be smaller than those for paths closer to the earth, as indicated in part (c) of Fig. 6; whistler patterns of this type can be discerned in Fig. 7. Thus, at any time N_e (r, $\theta_M = \pi/2$) decreases rather slowly until r reaches a critical radius. At this point an abrupt decrease in density is indicated, and beyond this knee in the ionization profile, N_e continues to decrease, with a steeper gradient than

in the inner region. The position of the knee varies with time and the equatorial boundary ranges from 3 R_e to beyond 6 R_e. It now appears that the previous agreement with $N_e \sim r^{-3}$ was only valid in a gross sense since it was derived by averaging the whistler densities over time without taking into account the existence and the motion of the knee.

Recent comprehensive reports by Carpenter and Angerami[22,23,24] summarized the results of the whistler analysis program, and the indicated density distributions are depicted in Fig. 8. The shaded region, in Fig. 8a, bounded by the L = 4 field line (i.e., that line with $r/R_E = 4$ at $\theta_M = \pi/2$) represents the high density plasma within the knee or "plasmasphere". Beyond the knee the densities fall below the solar wind densities (whistler analysis has yielded values of N_e as low as 0.5 electrons/cm^3 at $L \gtrsim 7.6$) and hence this may be called a plasma trough. Figure 8b shows that the knee is extremely sharp, especially in the post-midnight region, and equatorial density changes of almost two orders of magnitude in a distance of 0.15 R_e have been detected.

Within the knee, the density profiles appear to be consistent with a generalized form of a hydrostatic equilibrium model. In the case of a neutral, isothermal non-rotating atmosphere this would yield

$$N(r) \simeq N(r) \exp - \left[\frac{mg(r)}{\kappa T} - \frac{mg(r_o)}{\kappa T}\right] ,$$

$$\simeq N(r_o) \exp - \frac{z}{H} \qquad (8)$$

with $z = r - r_o$, and $H = \kappa T/mg(r_o)$ for $z << r_o$. In fact, the lower magnetosphere contains a combination of H^+, He^+, and O^+ ions, T_e and T_i may differ, the gravitational attraction over the dipole field line varies with r, and the centrifugal force varies with latitude. Even if we assume that the plasma is isothermal, the above complications require the introduction of individual scale heights for the different species, $H_i = \kappa T/m_i g(r_o)$, and the partial pressures are given in terms of Eq. (1) with

$$z(r,r_o) \rightarrow r_o \left[1 - \frac{1}{r} - \frac{\Omega^2 r_o}{2g(r_o)} \cos^2 \theta_o \, (r^2-1)\right] \tag{9}$$

where Ω is the earth's angular velocity and θ_o is the latitude of the field line at r_o (we again neglect the distinction between geomagnetic and geographic latitude). The resulting diffusive equilibrium distribution is a complicated function of $\vec{r}$, the base abundances and the scale heights, and charge separation effects enter because the electrons have a tendency to rise with respect to the heavier ions. However, if r is not too large, the centrifugal forces can be neglected and the final diffusive equilibrium distribution is approximately given by

$$N_e \sim \exp\,(K/r) \; . \tag{10}$$

Within the knee, the whistler results are in good agreement with this prediction for an isothermal atmosphere with $750°K < T_e < 3000°K$[24,25].

Beyond the knee a "collisionless" model appears to offer a valid description of the density profile. That is, the density is so low that collisions may be neglected, and the total energy of any individual particl

which includes kinetic, graviational, rotational, and electrostatic contributions remains constant. Moreover, in this collisionless region, the magnetic moment

$$\mu = \frac{m v_\perp^2}{B} \tag{11}$$

is a constant of motion associated with cyclotron rotation around the magnetic field line. Since B varies along any given L-shell, $v_\perp^2$ does the same, and the pitch angle, $\alpha = \sin^{-1}(v_\perp/v)$ is not constant. Many particles actually mirror at certain B-values along the L-shell and if we neglect gravitational, rotational, and electrostatic contributions, the pitch angle and field value at other points in the trajectory are then related by

$$\frac{\sin^2\alpha(\vec{r})}{B(r)} = \frac{1}{B_m} \tag{12}$$

where B_m is the magnetic field at the mirror point, $\alpha = \pi/2$. The collisionless distribution which takes into account all of these effects has been obtained by Eviatar, et al.,[26] and by Angerami[24]. If $T_e = T_i$ = constant, then N_e varies along a line of force or L-shell according to

$$\frac{N_e}{N_{eo}} = \exp\left[\frac{-z}{2H}\right] - \left[1-B/B_o\right]^{1/2} \exp\left[\frac{-z}{2H(1-B/B_o)}\right] \tag{13}$$

where $H = \kappa T/mg$, z is given by Eq. (9), and the subscript o refers to the base of the collisionless region. To a good approximation, the collisionless model can be represented by $N_e \sim r^{-4}$ for $r \lesssim 8\ R_e$.

These results have been verified and extended by analyzing the propagation characteristics of natural proton resonant magnetospheric emissions called micropulsations, or hydromagnetic whistlers[27,28,29,30]. In the frequency range $\omega \simeq \Omega_c$, the cold-plasma dispersion relation for parallel propagation in the mode $n^2 = L$ is[19]

$$n^2 \simeq \frac{\Omega_p^2}{\Omega_c(\Omega_c - \omega)} \tag{14}$$

and the group velocity is

$$V_g(\omega) \simeq c \frac{\Omega_c}{\Omega_p} \frac{[1-\omega/\Omega_c]^{3/2}}{[1-\omega/2\Omega_c]} \quad . \tag{15}$$

As $\omega \to 0$, $V_g \to V(\text{Alfven})$ and the higher frequency components travel more slowly, so that a sonogram trace will show bands with time delay increasing with frequency, in contrast to the whistler case. Figure 9 shows a hydromagnetic emission band which appears to be associated with a wave packet bouncing back and forth between hemispheres in the mode $n^2 = L$, with successive dispersions given by Eq. (15). Analysis similar to that described above identifies the path and yields $N_p(\vec{r})$. It appears that micropulsations propagate in the region near or beyond the knee ($L \simeq 5$-9) and the data confirm the existence of the plasma trough, with indicated densities ranging as low as 0.17 protons/cm^3 at $L \sim 7.5$, near the midnight meridian.

In general, local measurements support this picture of the plasma density profile. An unexpected and valuable technique for exploration of the distributions in the magnetosphere involves the generation of wave motions by transmitters carried on spacecraft. For instance, Alouette 1 (launched

on December 4, 1962) carried a powerful sounding transmitter and a sensitive receiver. The transmitter frequency was swept between 0.45 and 11.8 Mc/s, and the signals were to be reflected at altitudes with f(trans) = $f_p^{-}(h)$; by measuring the delay time for the echo, h would be determined. This topside sounding technique did give valuable information about $N_e(h)$ in the ionosphere, but it was difficult to make accurate measurements of the time delays near the Alouette orbit (h ≃ 1000 km). However, it was found that the high powered transmitter generated very strong plasma "resonances" near the spacecraft. More precisely, strong zero range reflections are obtained when the transmitted frequency equals the frequency of a local resonance (e.g., the plasma resonance at ω_p, cyclotron harmonics at $n\omega_c$, the upper hybrid resonance at $(\omega_c^2 + \omega_p^2)^{1/2}$, etc.) or a local cutoff (e.g., $\omega^2 - \omega\omega_c \simeq \omega_p^2$, etc.). These spikes are easily distinguished and the analysis of the Alouette 1 ionograms[31] has yielded fairly complete maps of $N_e(r,t, h \simeq 1000 \text{ km})$.

Near the L-shell identified with the knee, Alouette 1 generally appeared to detect a dip in the ionization density, but at higher latitudes, N_e would rise again, and no definite confirmation of the existence of a plasma trough was established. This situation was greatly clarified with the launch of Alouette 2 into an elliptical orbit which penetrated higher into the magnetosphere. It was found (J. Chapman, unpublished) that at 1500 km altitude the density in the polar and auroral region beyond the knee was less than 30 electrons/cm^3 a significant percentage of the time, and densities as low as 0.1 cm^{-3} were detected. Presumably, at somewhat

higher altitudes the low densities would appear more frequently, and the plasma trough would seem to be a permanent feature of the polar region at altitudes exceeding 2000-3000 km.

Spacecraft experiments designed to investigate the thermal plasma distributions in the outer magnetosphere by direct means have not all yielded entirely consistent results. Observations of knee effects in satellites and rockets date back to the work of Gringauz and his colleagues[32] who flew ion traps on Luniks 1 and 2 and noted significant decreases in positive ion currents at several earth radii. These observations have now been extended by Taylor[33] who measured H^+ and H_e^+ currents on OGO-1, and again the observed decreases in flux were consistent with the whistler indications of abrupt density decreases.

On the other hand, the retarding potential analyzer measurements of Serbu and Maier[34] on IMP 1 through 4 do not show abrupt decreases in j_+ or j_- at the knee, although the instrument is not very sensitive to positive ion currents. This disagreement is probably associated in some manner with the plasma sheath, about which little is known. However, some recent measurements illustrate that very complex phenomena can occur in the region surrounding a distant spacecraft, and these effects can degrade any attempt to observe very low energy particles, especially electrons: a) On Pioneer 6, Wolfe was able to determine (private communication) that a very dense sun-oriented photoelectron cloud continuously hovered in front of the illuminated portion of the spacecraft. Incident solar ultra-violet radiation apparently charged the sub-solar part of the spacecraft to

$e\phi \simeq +$ 10-15 volts, and this charge retained the photo-cloud. Thus, the Pioneer 6 surface was not an equipotential (this should be true in general since metallic surfaces are usually painted or wrapped in mylar for thermal balance), and one might expect this phenomenon to vary from spacecraft to spacecraft. Since the IMP retarding potential analyzer had +15 or +50 volts on its outer grid in the electron modes, these photoelectrons would be swept into the cup; b) It has been verified that solar cell panels produce electrostatic distributions which can affect the local flux determinations; c) Recent measurements on the U.S. Air Force spacecraft OV3-3[35] show that fringing fields from AC instruments can produce growing plasma oscillations (ion acoustic waves) in the ambient medium. Figure 10 illustrates the generation of external electrostatic waves with no magnetic components when the second grid (with respect to the outermost shielding grid) of the OV3-3 Faraday cup is modulated at 2 kc/s, and the absence of such interference when the fourth grid is similarly modulated. In each case several kilovolts is applied to the modulating grid, and the fringing field which escapes from the cup apparently exceeds the runaway field when the outer grid is excited. Since these waves appear to have finite growth and decay rates, any attempt to measure low energy electrons on a spacecraft which also carries an AC cup of the type shown (this includes OV3-3, IMP 1-4) may be seriously degraded, even if the measurements are not simultaneous; d) Finally, there is the question of the effective collecting area for a probe which measures j_- in the vicinity of the knee. The sheath size should be on the scale of the Debye length with $L_D = 6.9\ (T/N)^{1/2}$ cm.

If the temperature does not change significantly across the knee, then the results of Fig. 8 indicate that L_D^2 increases by a factor of about sixty as we go out, and the collecting "cone" for any given probe abruptly changes size in this region. All of these problems may have some bearing on the interpretation of low energy particle measurements in the outer magnetosphere; they do not necessarily involve the experiments of Serbu and Maier, but it must be realized that sheath phenomena do introduce serious uncertainties.

Another ground-based technique which attempts to obtain $N_e(r)$ in the distant magnetosphere is based on measurement of the differential travel time for RF signals (f = 25 Mc/s and 50 Mc/s) which are reflected from the lunar surface[36]. The preliminary results of this study yield an average density of about 100 electrons/cm^3 all the way to moon ($r \simeq 60\ R_e$) when the moon is in the geomagnetic tail. This result has been criticized by Dessler and Michel[37] and one source of great difficulty involves determination of the appropriate contribution to the time delay from the night side ionosphere and lower magnetosphere. The electrons in these regions may produce unexpectedly large time delays (D. Carpenter, private communication) and scattering from coherent plasma oscillations with scale sizes near the RF wavelengths can also introduce anomalous retardation[38].

4. ENERGETIC PARTICLES

The nearly dipolar configuration of the inner magnetosphere allows the possibility of durable confinement or trapping of energetic charged particles by a combination of periodic motions in the geomagnetic field. The first adiabatic invariant, μ, leads to mirroring at $B = B_M$, $\alpha = \pi/2$, and the particle can bounce back and forth between mirrors at opposite hemispheres. The action integral, J, is conserved, and a second, adiabatic invariant

$$I = \frac{J}{2p} = \frac{1}{2p} \oint p_{\parallel} ds$$

$$= \int_A^{A'} (1-B/B_M)^{1/2} \, ds \qquad (16)$$

is associated with the bounce motion; here p is the particle momentum and the integral is taken over a field line between mirror points A and A'. Particles also drift slowly in longitude around the earth because of the radial gradients and the curvature of the magnetic field. Protons drift to the west, electrons to the east, and the corresponding (third) adiabatic invariant is Φ, the total magnetic flux enclosed by the particle in one complete azimuthal drift.

The natural periods of these motions are very different. The periodicity associated with cyclotron motion is the gyroperiod, $\tau_1 = T_c = 2\pi mc/qB$, and for the earth's field a particle which mirrors on a given L-shell with equatorial pitch angle α_o and speed $v = \beta c$ has a bounce time given[39] approximately by

$$\tau_2 = (0.11 - 0.05 \sin \alpha_o)\, L/\beta \text{ seconds.} \qquad (17)$$

The period for drift completely around the earth is on the order of[39]

$$\tau_3 = 172 \frac{\gamma}{\gamma^2-1} \frac{1}{m_o L} \text{ minutes} \qquad (18)$$

where $\gamma = (1-\beta^2)^{-1/2}$ and m_o is the rest mass. Thus, in the region where the geomagnetic field is dipolar and steady, one may expect that energetic charged particles can be trapped until they undergo particle-particle or particle-wave collisions which eject them from their orbits.

The first satellites carried geiger counters and detected large fluxes of energetic trapped particles in what is called the Van Allen belt. Virtually every earth orbiting spacecraft since then has included in its payload one or more detectors capable of examining the distribution of these particles, and a tremendous amount of data has been accumulated since 1958. Despite this intensive exploration, relatively little order has become apparent and many fundamental problems remain. It is now clear that trapped particles are continually supplied and energized by some sources, and that many complex processes limit the trapping lifetimes. A great difficulty appears when one tries to analyze the results because the instantaneous distribution function at a given point is dependent on the previous history of the unidentified sources and sinks, the diffusion rates, and various internal acceleration processes in an unknown manner. Moreover, until very recently the particle counters flown most frequently were integral energy detectors measuring $j(E > E_o)$ (geiger counters,

scintillation counters, solid state detectors, ionization chambers) and detailed energy distribution functions could not be constructed. Additional problems with these detectors are associated with the difficulty of distinguishing between electrons, protons, and bremsstrahlung, and the lack of comparable sensitivity for measurement of electron and proton fluxes.

Nevertheless, these experiments have established that a relatively stable inner zone (centered at $L \sim 1.5$) contains very energetic trapped protons with $E \gtrsim 30$ Mev, while the most prominent particles in the "outer belt" ($L \simeq 3$-4) are electrons with $E \gtrsim 1.6$ Mev.[40] To a first approximation, all durably trapped particles lie within a toroidal region bounded on the earth side by a spherical surface with $h \sim 700$ km; the outer surface is roughly the L-shell with $L \sim 8$. Within this region, the energetic particle distributions are anisotropic. That is, particles mirroring at altitudes less than about 100 km are rapidly removed by atmospheric scattering, and at any higher altitude a loss cone exists, in which particles with pitch angles between zero degrees and

$$\alpha_D = \sin^{-1} [B(h)/B(h=100 \text{ km})]^{1/2} \qquad (19)$$

are absent in the steady state.

The inner Van Allen zone is quite stable, the outer belt population exhibits marked temporal variations (see Ref.(39, 40) for summaries and other references), and the non-dipolar outer magnetosphere and tail regions appear to contain distributions of non-trapped particles

with lower energy; O'Brien[41] has proposed that these particles which cannot drift completely around the earth be referred to as the auroral population. At present it is difficult to make very general statements about any of these groups, but this is especially true of the lower energy components. The considerable exploration which has been carried out with geiger counters, etc., reveals the presence of huge temporal and spatial fluctuations, especially in the outer magnetosphere. However, many of these changes undoubtedly represent very minor variations in the high energy tails of the distribution functions; any small compression or heating of an electron distribution with $\kappa T \sim 5$ kev can produce a dramatic change in the count rate of a geiger counter having an energy threshold of about 30-40 kev and a fixed background sensitivity determined by the cosmic ray flux.

Mapping of the lower energy magnetospheric component using a differential electrostatic analyzer is just beginning to be carried out. Figure 11 shows some partial electron energy spectra taken on OGO-3[42] in the evening part of the outer magnetosphere and tail regions. It can be seen that the electron spectra soften markedly with increasing distance, that very abrupt changes in flux are encountered, and that in these spikes the peak fluxes associated with the lower energies vary little with range. When the total electron energy density in a spike is computed, it is found that $N\kappa T$ is comparable to $B^2/8\pi$, and one may suspect that the entire outer magnetosphere and the tail have regions with β near unity.

Figure 12 shows low energy proton fluxes measured on OGO-3 in the same neighborhood[43]. Frank has found densities associated with these protons which are very nearly the ones predicted by the whistler measurements, and it appears that the hydrostatic pressure, $P = NkT$, varies little across the knee. At L = 6, Frank constructed a differential energy spectrum and found a peak flux near $E \simeq 6$ kev, but the distribution clearly had a non-Maxwellian tail. An extrapolation of these results fits well with the $E > 97$ kev proton fluxes measured earlier on Explorer 14 by Davis, et al.[44] In fact the composite proton spectrum has the same shape as the typical transition region proton spectrum[45], but all energies are higher. Since the peak fluxes are found near L-values which are related to the distance to the magnetopause boundary, it is tempting to speculate that the particles originate in the transition region, but unfortunately at this time these lower energy measurements which relate very directly to the plasma problems are quite incomplete and preliminary.

Several distinct sources contribute to the total energetic particle population of the magnetosphere. Solar and galactic cosmic rays produce neutrons when they interact with the earth's atmosphere, and decay of the neutron albedo within the geomagnetic field leads to trapping of very energetic protons and electrons. The high altitude nuclear tests also injected very significant fluxes of trapped particles, and at present the penetrating electron population in the inner belt is primarily a remnant of the Starfish explosion of July 9, 1962. These sources are thought

to account for the inner zone protons with E $\gtrsim$ 50-100 Mev, and perhaps the inner zone electrons with E $\gtrsim$ 1 Mev[40], although softer particle fluxes which exhibit large temporal variations are also detected in these regions, and other phenomena must be responsible for their presence. However, beyond L $\sim$ 2, the fluctuations of particle populations are closely associated with geomagnetic disturbances, and as noted above it seems likely that the energetic particle content of the outer belt, the outer magnetosphere, and the tail is directly associated with the huge energy flux delivered by the solar wind.

Various specific mechanisms for transferring this energy to the magnetosphere have been proposed. For instance, it has been suggested that solar wind particles themselves enter in the distant tail where reconnection with the interplanetary field occurs; if these particles migrate adiabatically toward the earth in the supposedly quiet tail E and B fields, then μ will be conserved so that the energy increases with B. Electrostatic acceleration of particles injected from the sunlit magnetosphere boundary on the neutral points has also been considered. Taylor and Hones[46] constructed a reasonable electrostatic potential system for the magnetosphere and they obtained a variety of numerical solutions for the adiabatic motion of charged particles in the nonuniform $\vec{E}$ and $\vec{B}$ fields.

The potential distribution is derived primarily from the ionospheric DS current patterns, assuming that the geomagnetic field lines are equipotentials. In addition a unipolar induction electric

field is inserted to account for the rotation of the inner geomagnetic field, the ionosphere, and the lower magnetosphere; this effect introduces a term

$$V(r,\theta_M) \simeq -\frac{1}{c}\,\Omega\mu_E\,\frac{\sin^2\theta_M}{r} \qquad (20)$$

where μ_E is the dipole moment of the earth and Ω is the angular velocity. The static acceleration contemplated involves conservation of μ, I, and $W = mv^2/2 + qV$. Particles gain energy (several tens of kilovolts) as they come into the strong magnetic field near the earth, and they are then either reflected [$B_M > B(h\tilde{=}100$ km)] or precipitated [$B_M < B(h\tilde{=}100$ km)]. Addition of weak non-conservative phenomena (fluctuations which violate the above adiabatic restriction) may certainly scatter many of these particles from the loss cone to the trapped region, but this effect can clearly go in both directions. Furthermore, although the static calculations could be relevant when one considers the behavior of the very soft particles, it is apparent that a substantial amount of energy resides in the electron component with E > 30-50 kev, and the proton component with E > 100 kev; some non-static energization mechanism must explain the presence of these higher energy particles, and their properties.

One very important energy source for the outer zone has been identified and analyzed in recent years. Kellogg[47] first suggested that long period electromagnetic or electrostatic fluctuations could violate the third invariant while the first and second remain conserved. Irregular changes allow diffusion of particles across L-shells, and there is an

associated increase in energy, W. For a dipole field,

$$[WL^3 \sin^2 \alpha]_{r=r_1} = [WL^3 \sin^2 \alpha]_{r=r_o} , \qquad (21)$$

where the subscript o refers to the conditions at the source and the cross-L motion is described by a Fokker-Planck equation

$$\frac{\partial F}{\partial t} = - \frac{\partial}{\partial r} \left[\left\langle \frac{\Delta r}{\Delta t} \right\rangle F \right] + 1/2 \frac{\partial^2}{\partial r^2} \left[\left\langle \frac{(\Delta r^2)}{\Delta t} \right\rangle F \right] . \qquad (22)$$

Parker[49], and Davis and Chang[50], evaluated the diffusion coefficients associated with impulsive changes in the solar wind flux. It was assumed that in a typical sequence the geomagnetic field is compressed on a time scale short compared to τ_3 for energetic particles [see Eq. (18)], with a subsequent slow decay [$\tau >> \tau_3$] and it was shown that a given initial energy distribution becomes broadened as it diffuses in L-space. Fälthammer[51] repeated these calculations for time varying electrostatic fields, and he noted that the basic mode of acceleration is a stochastic one in which both acceleration and deceleration occur. There are resonant frequencies corresponding to integral multiples of the azimuthal drift frequency, and even if the imposed field varies at random, some particles are accelerated, provided that the power spectrum overlaps the range of resonant frequencies.

Nakada and Mead[52] applied these theories using observed properties of sudden commencements and sudden impulses to evaluate the Fokker-Planck coefficients, and they estimated

$$\left\langle \frac{(\Delta r)^2}{\Delta t} \right\rangle \simeq 0.031\ r_{Bo}^{\ 2} \left[\frac{r}{r_{Bo}}\right]^{10} \frac{(\text{earth radii})^2}{\text{day}} \tag{23}$$

$$\langle \Delta r \rangle / \langle (\Delta r)^2 \rangle \sim 4/r \tag{24}$$

where r_{Bo} is the quiet-time subsolar magnetosphere boundary (on the order of 10 R_e). A more general Fokker-Planck equation with a term representing scattering in pitch angle and a loss term associated with charge exchange scattering was solved for the case of protons diffusing inward from the subsolar boundary under the action of storm impulses. A transition region source spectrum of the form exp $(-E/E_o)$ with $E_o \simeq$ 7-10 kev was assumed (representing the high energy tail of the transition region protons), and integral energy spectra for the range $2 < r/R_e < 7$ were computed. Figure 13 shows a comparison between this theory[52] and the experimental observations of Davis, et al.[44] It cannot be doubted that this kind of stochastic acceleration mechanism explains many aspects of the lower energy proton content of the magnetosphere, including fluxes observed on OGO-3. Indeed, in order to account for the observed steady fluxes, it is only necessary to assume that one part in 10^6 of the incident solar wind protons must be supplied to the magnetosphere via this process.

This mechanism can also induce acceleration and diffusion for electrons and some measurements show that the process does have importance

in the outer magnetosphere. For instance, Eq. (23) predicts a diffusion time which varies as L^{-8}, and Fig. 14 shows the actual velocity of inward radial motion for an outer radiation belt peak of E > 1.6 Mev electron densities as a function of L[53]; Frank fitted these Explorer 14 data with a power law, $v\alpha L^n$, and he found $n = 8(\pm 1)$. However, very large fluctuations in the electron sources apparently occur in contrast to the proton case, and study of the electron distributions reveals that other acceleration mechanisms must be operative as well as this one based on violation of the third invariant.

At least two other processes have been discussed. A "bounce" resonance is possible[54] in which the disturbance field power spectrum contains components at the bounce frequency, $2\pi/\tau_2$ and this can lead to acceleration (and dumping). Finally, higher frequency oscillations can produce stochastic cyclotron acceleration if the power spectrum contains components at Doppler shifted gyrofrequencies. Fredricks, et al.[55], considered the acceleration produced by electrostatic oscillations

$$m\ddot{\vec{r}} = -e\vec{E} + e\dot{\vec{r}} \times \vec{B}_o, \tag{25}$$

$$\vec{E} = -\vec{\nabla}\phi, \; \phi = \phi_o \int \cos\left[\vec{k}\cdot\vec{r} - \omega t - \psi(t,\omega)\right] g(\omega)\, d\omega \tag{26}$$

with $\psi(t,\omega)$ a stochastic phase variation, and it was shown that this acceleration process can be quite efficient. In particular, ion acoustic waves are slow, and almost any spectrum can readily be Doppler broadened to cover some electron cyclotron frequencies (for instance, if $N_e \simeq 500$ cm^{-3} at L = 5, $\theta_M \simeq \pi/2$,

then $f_c^- \lesssim 7$ kc/s and $f_p^+ \simeq 5$ kc/s) so that this mechanism appears to be a promising one.

Analysis of the energization problem is intimately associated with study of various precipitation phenomena, and in this area much information of value with respect to laboratory confinement studies may be at hand. It appears that on L-shells below about 1.25, atmospheric scattering is the dominant loss mechanism for high energy particles, but beyond this region the mechanism becomes too weak to be responsible for the observed steady loss rates. Dungey[56] and Cornwall[57] first suggested that pitch angle scattering due to cyclotron resonant interactions with discrete natural whistlers might govern the loss of trapped electrons above $L \lesssim 1.7$, but Roberts[58] noted that the observed pitch angle distributions and the observed variation of loss rate with energy both disagree strongly with the predictions of this theory (assuming that the spectral intensity of discrete magnetospheric whistlers falls rapidly above 10 kc/s). However, very rapid fluctuations in the rate of precipitation of E > 40 kev electrons observed directly on Injun 3[59] and indirectly, by detecting X-ray bursts[59], are consistent with the explanation that pitch angle scattering into the loss cone is associated with the gyrofrequency resonance.

A modified form of the whistler interaction theory was recently developed by Kennel and Petschek[60], and by Cornwall[61]; it involves an instability mechanism which appears to explain some features of the observed continuous precipitation. If we use the notation of Stix[19] and consider

the mode $n^2 = R$, then for $\omega < \omega_c$, $\omega_p/\omega_c >> 1$, Eq. (7) yields

$$\frac{c^2k^2}{\omega^2} \simeq \frac{\omega_p^2}{\omega(\omega_c-\omega)} \tag{27}$$

for the real part of ω, and the growth rate, γ, is given by linear perturbation theory as

$$\gamma = \frac{2\pi^2\omega_c^2}{k}\left(1-\frac{\omega}{\omega_c}\right)^3\left[A^-(V_R) - \frac{\omega}{\omega_c-\omega}\right]\int_o^\infty v_\perp dv_\perp\, F(v_\perp, v_\parallel = V_R), \tag{28}$$

$$A^-(V_R) = \frac{\int_o^\infty v_\perp dV_\perp \left(v_\parallel \frac{\partial f}{\partial v_\perp} - v_\perp \frac{\partial F}{\partial v_\parallel}\right)}{2\int_o^\infty v_\perp dv_\perp f}\,. \tag{29}$$

Here f is normalized to unity and is assumed to have axial symmetry about the magnetic field, the subscripts on v refer to direction with respect to $\vec{B}$, and the parallel velocity $V_R = (\omega-\omega_c)/k$ is the one which leads to a Doppler shifted cyclotron resonance.

For an isotropic distribution, any wave is damped at all frequencies, but if the velocity space distribution is anisotropic, there is always a band of frequencies which is amplified, as discussed by Harris[62]. Cornwall and Kennel and Petschek noted that the magnetospheric distributions are indeed anisotropic because of the existence of a loss cone. If, for instance, we consider a simple anisotropic distribution with $f(v_\parallel, v_\perp) = F(v, \alpha) = F_o(v) \sin^m \alpha$, then A^- is simply $m/2$, and all waves with

$$\frac{\omega}{\omega_c-\omega} < \frac{m}{2} \tag{30}$$

are amplified (this term is used to describe the growth because at present it is not clear whether the instability is convective or non-convective).

The quasi-linear theory was applied by Kennel and Petschek to estimate the effect of finite electron whistler mode noise on the electron population. A Fokker-Planck equation for diffusion in pitch angle was considered and the diffusion coefficient, $D = \langle(\Delta\alpha^2)\rangle / \Delta t$ was evaluated as

$$D = \frac{\omega_c^2}{v|\cos \alpha|} \left(\frac{B_k}{B}\right)^2 \tag{31}$$

where B is the ambient steady field, and $B_k^2 = B'^2 \Delta k$. Here B' is the noise amplitude and Δk is the width of the narrow wave number band near resonance which produces pitch angle changes $\Delta\alpha$ in time Δt. This theory predicts a continuous precipitation, and observed lifetimes for 40 keV electrons were used to estimate the required wideband noise levels. Kennel and Petschek proposed that whistler mode background levels on the order of $10^{-2}\gamma$ $(4 < L < 7)$ would be adequate to account for the precipitation rates observed on Injun 3, and experiments designed to investigate the background amplitudes are presently in orbit.

This instability can actually produce an upper limit on stably trapped particle fluxes since the growth times given by Eq. (28) depend on the value of $B^2/8\pi NKT$; large densities yield extremely rapid wave growth and hence large losses. Kennel and Petschek presented evidence that soft $(E \simeq 40\text{-}100$ kev) electron fluxes are indeed nearly always limited at about

the appropriate levels, however more energetic electrons (say E > 230 kev) have variable flux values with peaks well below the hypothetical threshold. This is not totally unexpected, since the sources for very energetic particles are considerably weaker, and moreover the whistler mode diffusion phenomenon is a resonant one; hence various energy groups will react in different ways to a given broadband noise signal. Some recent and very limited measurements[63] have established a weak correlation between the appearance of electrostatic noise signals and precipitation of E > 400 kev electrons. If future experiments confirm this relation, then it would appear that a non-resonant analog of Bohm diffusion might allow energetic particles to diffuse across L-shells and escape into the atmosphere, at least near the inner edge of the belts.

5. WAVES IN THE MAGNETOSPHERE

As discussed above, the study of wave modes in the magnetosphere is of interest because the oscillations can interact strongly with individual charged particles, and furthermore the analysis of wave characteristics provides an excellent plasma diagnostic. In the near future this last aspect will be explored in considerable detail. Investigation of the types of waves which actually exist or propagate in the magnetosphere can yield fundamental information about the microscopic stability of the plasma, the distribution functions, Landau and cyclotron damping or overstability, nonlinear wave growth, and wave-particle or wave-wave interactions.

The apparently simple problem of natural whistler propagation is one which has received a great deal of attention, and it now seems that various complex plasma processes combine to produce the orderly characteristics shown in Fig. 7. In Storey's original work[18] it was suggested that the striking guidance along the magnetic field (sometimes involving ten or more successive echoes with little attenuation) might require the existence of ducts, or field-aligned columns of enhanced ionization. Smith[64] examined the guidance associated with some specific forms of ducts, and he showed that trapping will generally not occur for frequencies higher than f_c^- (Min)/2 = f_c^- ($\theta_M = \pi/2$)/2. Whistlers which propagate down to the earth on field lines well within the knee do have sharp upper cutoffs with f (cutoff) approximately bounded by f_c^- ($\pi/2$)/2, and this duct-escape theory may, in fact, account for the guidance and the absence of higher frequencies

in these regions. On the other hand, Scarf proposed[65] that the cyclotron damping associated with an isotropic electron thermal distribution could provide sufficiently strong attenuation to explain some observed cutoffs. This theory was applied by Liemohn and Scarf[20] to a set of experimental data and it was shown that significant fluxes of 500 eV to 2 keV electrons would have to be present to provide adequate Doppler broadening.

It now seems that a mixture of these theories, supplemented by instability considerations, must be used to explain the observations, especially near and beyond the knee. Liemohn[66] generalized the cyclotron damping theory by considering the interaction between a whistler mode wave and an anisotropic electron velocity distribution. The growth rates were computed using the relativistic analog of Eq. (28), (29) and the distribution function was decomposed into a thermal part ($T \simeq 1250°K$) plus a high energy tail with $F\ (High) = G(E)\ H(\alpha)$. Forms such as

$$G \simeq E^{-n-1/2},\quad 1 \leq n \leq 3$$

$$H \simeq \Theta\ (\alpha_o - \alpha_D)\ \sin^M \alpha_o, \tag{32}$$

were considered; here α_o is the equatorial pitch angle, Θ is a smoothed step function and α_D is an ad-hoc cutoff ($\alpha_D \simeq 10°$) introduced to take into account the loss cone associated with atmospheric scattering. All numerical calculations were carried out for a boundary value problem with ω real, $k(\omega) = k_r + ik_i$, and the total amplification or attenuation coefficient was computed by evaluating

$$A(\omega)(db) = -10 \ln_{10} [2 \exp \int_{path} k_i(\omega,s)ds]. \quad (33)$$

Some typical results are shown in Fig. 15, with $A < 0$ representing attenuation associated with conventional cyclotron damping, and $A > 0$ representing growth. The transformation from attenuation to growth occurs when the Cerenkov radiation overwhelms cyclotron damping, and this transition can be quite steep for a resonant type of interaction in which a large number of particles absorb or emit wave energy. The experimental observations are in agreement with Fig. 15 in the sense that the whistler intensity seems to increase with frequency until the abrupt cutoff, with very heavy attenuation beyond this point. Furthermore, the OGO-3 results of Frank [see Fig. 11] show that large numbers of 0.5 - 2 keV electrons are present beyond the inner magnetosphere; if the distribution frunctions have loss cones as expected, then this instability should provide amplification of the original whistler impulse.

Independent evidence supports the idea that whistler propagation is associated with one or more plasma instabilities. Several of the spectrograms in Fig. 7 exhibit triggered emissions arising from the vicinity of the steep upper frequency cutoff, suggesting that the wave-particle interactions have disturbed the delicate balance between Cerenkov radiation and cyclotron damping. Moreover, as Liemohn noted[66], many multiple-hop VLF whistlers have amplitudes which increase in the first few echoes. Indeed, it may be that "ducting" frequently represents local amplification of wave components with $\vec{k}$ parallel to $\vec{B}$, rather than trapping in an actual field-aligned density enhancement.

Lightning strokes do not directly produce magnetospheric VLF noise impulses in the mode $n^2 = L$. This is so because the positive ion concentration in the upper ionosphere ($200 < h < 1500$ km) is a mixture of O^+, H_e^+, and H^+, with $m_{eff} \simeq 16$ near the bottom of this range and $m_{eff} \sim 1$ near the top. Waves with $\omega < \Omega_c(O^+)$ injected into the base region can propagate through, but in a multicomponent plasma, new cutoffs with $n^2 = L = 0$ appear, and between the appropriate resonance ($n^2 = L = \infty$) and the next higher cutoff, only the mode $n^2 = R$ can propagate[67]. However, ion gyrofrequency phenomena have been observed on satellites in association with ordinary electron whistler signals. These waves are called ion cyclotron whistlers and Fig. 16 shows the sonogram of a proton whistler observed on Injun 3[68]. The explanation for this phenomenon is contained in the equations for wave propagation in a cold magnetized plasma; if we use the notation of Stix (Chapter 1, Reference 19), then

$$D = (R-L)/2 = 0 \tag{34}$$

defines crossover frequencies in which both transverse modes are linearly polarized. Strong coupling between right and left hand circularly polarized waves can take place as they propagate past a localized region with $D = 0$, and polarization reversal may occur. For $\omega << \omega_c$ and $\alpha = N(H^+)/N_e$, $\beta = N(H_e^+)/N_e$, $\gamma = N(O^+)/N_e$, the condition $D = 0$ is approximately

$$1 = \frac{\alpha}{1-[\omega/\Omega_c(H^+)]^2} + \frac{\beta}{1-[\omega/\Omega_c(H_e^+)]^2} + \frac{\gamma}{1-[\omega/\Omega_c(O^+)]^2} . \tag{35}$$

If there is only one ionic species Eq. (35) has no solution, but for α, β, and γ finite, there are two real solutions at ω_{12} $[\Omega_c(H^+) > \omega_{12} > \Omega_c(H_e^+)]$ and ω_{23} $[\Omega_c(H_e^+) > \omega_{23} > \Omega_c(0^+)]$. Thus, the noise signal which enters a region having D = 0 in the right hand mode, emerges with part of its energy in the mode $n^2 = L$. This is shown in Fig. 16 [here $\Omega_1 = \Omega_c(H^+)$ and Ω_c represents the maximum frequency along the path for which polarization reversal can occur].

Analysis of proton and helium whistlers yields α, β, and γ so that these signals provide a powerful and accurate diagnostic for investigation of the abundance ratios in the lower magnetosphere. More recently, Gurnett and Brice demonstrated[69] that the attenuation of proton whistlers is undoubtedly due to cyclotron damping from an isotropic thermal proton distribution. Thus, this mechanism, originally proposed by Scarf for natural whistlers and micropulsations[65][70], has application to ion cyclotron whistlers and leads to determination of the local ion temperature.

The wave mode associated with the natural geomagnetic micropulsations shown in Fig. 9 is definitely the mode with $n^2 = L$, and we assume that this statement is valid in general (some early literature on this subject contains speculations that micropulsations have $n^2 = R$; this appears to be incorrect in most, if not all, cases). Several possible generation mechanisms for these "hydromagnetic whistlers"[27] have been considered, but at present the source is not positively identified. The most natural explanation is that the proton distribution is anisotropic in the outer

magnetosphere. The growth rate analagous to that of Eq. (28) is

$$\gamma = \frac{\pi^2 \Omega_c^3}{k\omega} \frac{(\Omega_c - \omega)^3}{(\Omega_c - \omega/2)} \left[A^+(V_R) - \frac{\omega}{\Omega_c - \omega} \right] \int_0^\infty v_\perp dv_\perp \, f^+(v_\perp, v_{||} = V_R) \quad (36)$$

where A^+ is defined as in Eq. (29) with $f^- \rightarrow f^+$, and V_R is now $V_A (1-\omega/\Omega_c)^{3/2} \Omega_c/\omega$ (V_A is the Alfvén speed). Cornwall[61] and Liemohn[66] computed micropulsation growth rates for various reasonable proton distributions, and Cornwall speculated that hydromagnetic whistlers might limit the proton content in the magnetosphere in much the same way as electron whistlers may limit the electron population. A disturbing feature of this theory is that it does not offer an obvious explanation for the pulse-like nature of the observed emission. Cornwall suggested that the discreteness of the signals might be associated with non-linear self-quenching effects. However, these characteristics may also arise if, for instance, the natural discrete micropulsations are generated by interactions in which a beam of trapped protons emits Cerenkov radiation so that finite hydromagnetic wave pockets bounce back and forth between hemispheres. As noted above, the origin of these noise signals is not known with certainty, at present.

Some other magnetospheric wave modes have been identified unambiguously. Large amplitude ground level magnetic disturbances which are eliptically polarized have been shown to be hydromagnetic waves[71], and similar extremely low frequency oscillations are observed by spacecraft magnetometers[72]. It is believed that these waves are somehow associated with variations in the solar wind pressure. Flute instability of the magnetopause boundary might provide a source[73], or unstable low frequency fluctuations in the wind itself[74] could be triggered into rapid growth in the transition region.

At least one electrostatic mode was detected with the long electric sounder antennas of Alouette (but not with the loop antenna of Injun 3). A VLF hiss band has a low frequency cutoff related to the local lower hybrid resonance[75]. These emissions can be triggered by whistlers or other atmospheric noises, and enhanced intensities appear near the whistler knee (D. Carpenter, private communication). However, the Alouette VLF experiment was not designed to be efficient in the detection of short wavelength electrostatic oscillations; the sounder antennas are 46 meters in length and a long wavelength electromagnetic wave with moderate or low amplitude can mask an oscillation with $\lambda \sim L_D$ (centimeter to meters in the near magnetosphere). Moreover, the low impedance input circuit on Alouette can conceivably respond to the magnetic component of an electromagnetic wave, and this may also degrade the sensitivity with respect to plasma oscillations.

Very different kinds of VLF electric field experiments were flown on the USAF satellites 1964-45A and OV3-3 (1966-70A). Short antennas with small collecting areas (to minimize charging currents) were coupled to high impedance preamplifiers with capacitive voltage dividers (see Refs. 35, 63). The resulting electrometers are essentially AC Leyden jars and they have detected ambient large amplitude electric fields which appear to represent plasma oscillations (see Fig. 10). On OV3-3 simultaneous E,B measurements are made, along with instantaneous on-board (E,B) correlations, and the majority of the signals seem to be electrostatic. At frequencies above all ion gyrofrequencies the electric fields are primarily oriented along $\vec{B}$.

It has been conjectured that these observations are associated with ion acoustic waves having $\vec{E} = -\vec{\nabla}\phi$, $\phi = \phi_o \cos(k\cdot r - \omega t)$. If the damping can be neglected then

$$\frac{1}{\omega^2} \simeq \frac{M_i}{k_{//}^2 \kappa T_e} + \frac{1}{\Omega_p^2}, \quad 0 < k = k_{//} < K_D . \tag{37}$$

On OV3-3 a broad-band channel (20 c/s to 100 c/s) also supplies data in the frequency ranges near and below the local H^+, H_e^+, and O^+ gyrofrequencies, and in this range hiss bands and discrete electrostatic waves with a variety of polarizations and dispersions are detected. Some of these may still be ion acoustic waves since Eq. (37) is derived from

$$\frac{1}{\omega^2} \approx \frac{M_i}{k_{//}^2 \kappa T_e} + \frac{1}{\Omega_p^2}\left(1 + \frac{k_\perp^2}{k_{//}^2}\right) + \frac{k_\perp^2}{k_{//}^2}\frac{1}{(\Omega_c^2 - \omega^2)} + \ldots \tag{38}$$

and at sufficiently low frequencies $\vec{k}$ need not be parallel to $\vec{B}$[19]. Other possibilities for some of these discrete emissions are ion-ion hybrid frequencies or ion cyclotron harmonics which satisfy dispersion relations such as[19]

$$\omega^2 \simeq (2\Omega_c)^2 + \frac{\Omega_p^2 k^2 \kappa T \sin^4\theta}{M_i\left[\Omega_c^2 - \frac{\Omega_p^2}{12}(4 - \cos^2\theta)\right]}$$

with $\vec{k}\cdot\vec{B} = kB\cos\theta$. Sonograms are presently being analyzed in an attempt to identify these wave modes.

Large amplitude field-aligned electrostatic waves with $\omega > \Omega_c$ were also apparently detected on the Japanese sounding rocket, L-3-2, at altitudes above 150 km.[76] Another technique which yields information about magnetospheric plasma oscillations involves study of ground-based radar backscatter. Large scattering occurs when the density fluctuation scale size equals $\lambda\,(RF)/2$,[38] and enhanced cross-sections should appear at $(\omega \pm \omega_p)$ with an incident wave of frequency ω. Perkins, et al.[77] recently detected greatly enhanced backscatter at the electron plasma "lines".

The observed electrostatic wave fields at low altitudes have very large amplitudes. Although the present measurements are relatively crude and uncertainties involving the effective lengths and sheath corrections remain, it appears that the indicated VLF field strengths range from more than 10^{-5} volts/meter to 10^{-1} volts/meter in regions where $\kappa T/e \equiv 200$ millivolts and $L_D \sim 0.1\text{-}5$ cm. In an equilibrium plasma, a generalized equipartition relation for the distribution of thermal and electrical energy yields the expression for the background electrostatic energy,[78]

$$\frac{\langle \delta E^2 \rangle}{8\pi} = 2\pi n e^2 \sum_\alpha \int d^3k\, d^3v\, d\omega \, \frac{f_\alpha(\vec{v})\,\delta(\vec{k}\cdot\vec{v}-\omega)}{k^2 \left|\kappa(\vec{k},\omega)\right|^2} \tag{40}$$

where the sum is taken over all species and κ is the longitudinal dielectric constant,

$$\kappa(\vec{k},\omega) = 1 - \sum_{\alpha} \frac{\omega_p^2}{k^2} \vec{k}\cdot\int d^3v \vec{\nabla}_v f_\alpha \, (\vec{k}\cdot\vec{v}-\omega)^{-1}, \quad \mathrm{Im}\omega > 0, \tag{41}$$

The background fields in the magnetosphere generally appear to be significantly higher than is predicted by Eqs. (40), (41), and one must try to identify the mechanisms which yield the enhancements.

Perkins and Salpeter suggested[79] that the high energy tail of photoelectrons in the ionosphere could account for the large electron plasma oscillation levels observed by radar backscatter. As Tidman has shown,[80] a non-Maxwellian electron distribution such as

$$f = \frac{\beta}{(2\pi)^{3/2}V_e^3} \exp\left(-\frac{v^2}{2V_e^2}\right) + \frac{(1-\beta)}{(2\pi)^{3/2}V_E^3} \exp\left(-\frac{v^2}{2V_E^2}\right) \tag{42}$$

with $0 < (1-\beta) \ll 1$ and $V_E^2 \gg V_e^2$ has

$$\frac{\langle \delta E^2 \rangle}{\langle \delta E^2 \rangle_{\text{Thermal Eq.}}} \simeq \left(\frac{V_E^2}{V_e^2}\right) / \log[V_E/V_e(1-\beta)] \tag{43}$$

where

$$\frac{\langle \delta E^2 \rangle}{8\pi}_{\text{Thermal Eq.}} \simeq \frac{1}{(2\pi)^3} \int d^3k \, \frac{(\kappa T_e)K_D^2}{2(k^2+k_D^2)} \tag{44}$$

if the magnetic field is neglected.

For $V_E \sim 20\ V_e$ and $\beta = 0.9$, the high energy tail produces an enhancement of about two orders of magnitude in the electrostatic energy density.

In this connection, Fig. 17 shows a relatively unusual electron event observed by Frank on an inbound pass of OGO-3[42]. Here the double peak again strongly suggests that the excess of electrons with speeds greater than $(2\kappa T_e/M_e)^{1/2}$ should lower the net Landau damping and produce enhanced plasma oscillation levels. Indeed, the spectrum at 19:24 UT is so steep, that the stability of the distribution might be questioned. However, these measurements are unidirectional and it is impossible to evaluate stability without detailed angular information. Some evidence suggests that here the plasma is stable; in the sequence of Fig. 17 the apparent "thermalization time" is on the order of minutes while $T_p = 2\pi/\omega_p \simeq$ milliseconds. But even so, no definite conclusions can be drawn. A steady local source of fresh high energy particles may be present and the spacecraft motion of several kilometers per second thoroughly mixes temporal and spatial variations. A further complicating factor in any analysis of plasma phenomena in the geomagnetic tail is associated with the fact the Debye length is not always negligible compared to Larmor radii throughout this region. Chang[81], Coppi, et al.[82] and others have noted that finite Larmor radius effects play an important role in determining the structure and content of the tail and neutral sheet, which resembles a

natural stabilized pinch. At present, further detailed speculation about this tail region, which is obviously quite complex and relatively unexplored, seems unwarrented.

Closer to the earth, many plausible sources of large amplitude plasma oscillations may be enumerated. For instance, Eq. (32) describes a particle distribution function which will yield large field levels for two reasons: a) the high energy tail contributes many particles with speeds greater than the wave speed and this again leads to enhanced background levels; b) the velocity space anisotropy in the $H(\alpha)$ factor can produce a generalized form of two-stream instability. In the magnetosphere $\Omega_p >> \Omega_c$ and the analog of the electrostatic Harris instability[62] is the high frequency Rosenbluth-Post instability[83], which leads to oscillations near $\omega \simeq \Omega_p$ when particles are confined in a mirror geometry with a loss cone. For a situation in which a significant number of high energy tail particles with loss cones coexists with an isotropic low energy group, the growth rates and stability thresholds depend in detail on the forms of the electron and positive ion distributions; Chang[81] showed that quite large growth rates may be anticipated in parts of the magnetosphere.

A more conventional type of two-stream instability is associated with counterstreaming groups of particles. In the ionosphere, large amplitude plasma oscillations detected by radar backscatter (the equatorial electrojet, the radar aurora) were identified as field-aligned ion acoustic

waves, and at these altitudes collisions are still important. Buneman[84] and Farley[85] showed that electrons streaming across field lines could generate the ionospheric plasma oscillations by collisional or "viscous" coupling with the neutral population.

In the collisionless regions at higher altitudes, two-stream instabilities may be driven by D.C. electric fields associated with fluting. The question of mhd stability of the magnetosphere is an old one, and the interchange process is involved in formation of the geomagnetic tail, and in considerations of magnetopause stability. Recently, however, interest in the overall flute stability of the magnetosphere proper has been greatly intensified, as more details of the particle distributions have become available.

The geomagnetic field falls off rapidly with distance, and trapped particles experience an outwardly-directed force associated with motion in the curved field. Under these circumstances fluting is certainly possible and two separate problems are relevant; a) analysis must be performed to see if the system is energetically stable ($\delta^2 W > 0$) with respect to interchange; b) for a nominally unstable system, the currents which flow through the conducting ionosphere (end plates) must be examined to see if they can neutralize the electrostatic potential differences on a time scale sufficiently short compared to the flute growth time constant to stabilize the interchange. Extensive calculations on this problem were recently carried out by Chang, Pearlstein, and Rosenbluth[86], and Swift[87] also analyzed the situation from this point of view. Chang, et al.

considered an equatorial distribution function of the form

$$f_o\ (L,\ \theta_M = \pi/2,\ \alpha_o,\ E) =$$

$$C\ \delta\left(E - \frac{E_o}{L^a}\right) \frac{1}{L^b}\ (\sin\ \alpha_o)^P \tag{45}$$

and they showed that the marginal stability condition is

$$\frac{d}{dr}\ [(N\kappa T)\ V^\gamma]\ =\ 0, \tag{46}$$

where V, the volume of a flux tube, is proportional to L^4, $\gamma = \gamma(P)$ depends on the pitch angle distribution, and $5/3 < \gamma \leq 7/4$. For the population described by Eq. (45), $\delta^2 W$ vanishes when $(a+b) \gtrsim 6.5$ $(P \simeq 1)$, $(a+b) \to 7$ $(P \gg 1)$. The rapidly rising volume of the flux tube with increasing L plays a significant stabilizing role, and if, for instance, N_e actually varied as L^{-3} with $\kappa T_e \sim$ constant, then the low energy plasma distribution would clearly be stable. However, the thermal plasma density does not fall off smoothly with distance, and Scarf, et al.[88] noted that the knee density profile yields density gradients which exceed the critical pressure gradients, as shown in Fig. 18. If the electron temperature did not climb rapidly beyond the knee (i.e., if b were not negative), then the knee region would be continuously unstable with respect to interchange.

The preliminary OGO-3 results of Frank suggest that κT_e, κT_p do, in fact, rise very significantly in the region of the knee, and $d(N\kappa T)/dr$

appears to be small enough to yield $\delta^2 W \geq 0$ in the steady state. However, no quantitative analysis of this relationship has been made at present. Furthermore, since the thermal distribution within the knee and the energetic particles in the outer magnetosphere are derived from different physical sources, it may be anticipated that $\delta^2 W < 0$ will at least appear as a transient phenomenon. Indeed, for some reasonable energetic particle distributions, such as [39]

$$f_o(L,E,\alpha_o) = \frac{C_o \exp\ (C_1 L^5 E)}{E^{1/2}} \sin^3 \alpha_o \ , \tag{47}$$

the flute is energetically possible in the steady state.[86]

In this case, any potential difference between two geomagnetic field lines will drive currents down one field line, through the conducting ionosphere, and up another field line, as shown in Fig. 19. Chang, et al. considered line-tying stabilization by the resistive ionosphere, and they argued that even with distributions such as that of Eq. (47), the magnetosphere will generally be stable with respect to interchange. On the other hand, Swift and Scarf, et al.[63] observed that D.C. electric fields parallel to $\vec{B}$ which exceed the runaway field,

$$E_R = \frac{m}{e} \nu \left(\frac{\kappa T_e}{m}\right)^{1/2}$$

$$\simeq 10^{-6}\ (N/T)\ \log\ [10^4 (T^{3/2}/N^{1/2})] \tag{48}$$

[N is measured in cm^{-3}, T in degrees Kelvin, and E in volts/meter] produce ion acoustic oscillations by the Cerenkov mechanism. This establishes a finite, and reasonably small, magnetospheric conductivity parallel to the field lines, and reduces the line-tying associated with the neutralizing currents. Swift speculated that this effect could temporarily insulate the magnetosphere and allow extremely large electric fields to build up, with a subsequent catastrophic "discharge" resulting in the production of energetic particles.

This type of phenomenon appears to be operative in the auroral region. Large numbers of particles are rapidly energized and precipitated into the ionosphere at high latitudes[39]. Figure 20 shows some examples of auroral measurements from the satellite Injun 3[89]. At latitudes below about 60°, the 40 keV electrons are primarily trapped, since the flux of mirroring particles ($\alpha \simeq 90°$) greatly exceeds the downward precipitating flux ($\alpha \simeq 0°$). However, near 65° latitude the situation changes. The flux in each detector increases, and the downward flux approaches, or perhaps exceeds, the flux of mirroring particles. O'Brien observed[39] that these results, and those from other auroral experiments, could be simply explained by postulating the temporary presence of electric fields parallel to $\vec{B}$. This in turn might naturally be related to a flute instability, and indeed soft electrons (E > 10 keV) are frequently dumped just beyond this boundary. Gurnett showed that the VLF magnetic noise (auroral hiss) is related to the presence of the soft electrons[89], but no comprehensive measurements of electrostatic waves in these regions are available at present.

Some other theories of the aurora are based on the premise that the bombarding particles are energized elsewhere in the magnetosphere[46][82], but recent rocket measurements of local proton-electron anticorrelations seem to indicate that temporary (or extremely low frequency) electric fields with $E_{\parallel} \simeq 10^{-3}$-$10^{-1}$ volts/meter are indeed present in the auroral zone[90]. In fact, pitch angle distributions of 100 keV electrons obtained when Explorer 14 was in the distant night-side magnetosphere[91] also suggest that electric fields parallel to $\vec{B}$ may be important far from the earth.

These considerations indicate that study of wave-particle processes in the magnetosphere can illuminate some very basic characteristics of collisionless plasmas. Unfortunately, no direct measurements of $E_{\parallel}$ have been made to date, and the experimental study of magnetospheric waves is also quite incomplete. Moreover, fast measurements of the particle fluxes, which might allow the observer to discriminate between local electromagnetic or electrostatic oscillations and those which have propagated from distant sources, are completely lacking. However, the simple mapping of the magnetosphere is now on its way to completion. In the next few years we may expect to see more detailed use of the magnetosphere as a natural laboratory in which microscopic plasma physics can be studied from an internal platform which, hopefully, does not disturb the medium to be measured.

ACKNOWLEDGMENTS

I am grateful to many of my colleagues for information and helpful discussions, and to the authors who have allowed me to use information and figures from their reports and papers. I am especially indebted to Dr. L. A. Frank for communicating his recent results to me in advance of publication, and for his generous permission to reproduce some of the data here. This work was partly supported by the National Aeronautics and Space Administration under Contract NASW-1366.

REFERENCES

1. Chapman, S., and V. C. A. Ferraro, Terr. Mag. Atmos. Elec. 36, 77, 171 (1931), 38 (1933, 45, 245 (1940).

2. Parker, E. N., Astrophys. J., 128, 664 (1958).

3. The Solar Wind, ed. R. J. Mackin, Jr. and M. Neugebauer (Pergamon Press, 1966).

4. Wolfe, J. H., R. W. Silva, and M. A. Myers, J. Geophys. Res., 71, 1319 (1966).

5. Axford, W. I., p. 231, Ref. 3.

6. Lees, L., A. I. A. A. Journal, 2, 1576, 1964.

7. Mead, G. D., and D. B. Beard, J. Geophys. Res., 69, 1169 (1964).

8. Mead, G. D., J. Geophys. Res., 69, 1181 (1964).

9. Midgely, J. E., J. Geophys. Res., 69, 1197 (1964).

10. Piddington, J. H., J. Geophys. Res., 65, 93 (1960).

11. Dungey, J. W., J. Geophys. Res., 70, 1753 (1965).

12. Axford, W. I., H. E. Petschek, and G. L. Siscoe, J. Geophys. Res., 70, 1231 (1965).

13. Dessler, A. J., J. Geophys. Res., 69, 3913 (1964).

14. Ness, N. F., C. S. Scearce, and S. Cantarano, J. Geophys. Res., 71, 3305 (1966).

15. Ness, N. F., J. Geophys. Res., 70, 2989 (1965).

16. Speiser, T. W., and N. F. Ness, Goddard Space Flight Center Report X-612-66-290 (June, 1966).

17. Lin, R. P., and K. A. Anderson, J. Geophys. Res., 71, 4213 (1966).

18. Storey, L. R. O., Phil. Trans. Roy. Soc. London, A246, 113 (1953).

19. Stix, T. H., The Theory of Plasma Waves (McGraw-Hill Book Co., 1962).

20. Liemohn, H. B., and F. L. Scarf, J. Geophys. Res., 69, 883 (1964).

21. Carpenter, D. L., J. Geophys. Res., 68, 1675 (1963).

22. Carpenter, D. L., J. Geophys. Res., 71, 693 (1966).

23. Angerami, J. J., and D. L. Carpenter, J. Geophys. Res., 71, 711 (1966).

24. Angerami, J. J., Stanford Electronics Lab. Rept. No. 3412-7 (May 1966).

25. Angerami, J. J., and J. O. Thomas, J. Geophys. Res., 69, 4537 (1964).

26. Eviatar, A., A. M. Lenchek, and S. F. Singer, Phys. Fluids, 7, 1775 (1964).

27. Obayashi, T., J. Geophys. Res., 70, 1069 (1965).

28. Wentworth, R. C., Lockheed Missiles and Space Company Technical Report 6-75-65-11 (March 1965).

29. Watanabe, T., J. Geophys. Res., 70, 5839 (1965).

30. Dowden, R. L., and M. W. Emery, Plan. and Space Scie., 13, 773 (1965).

31. Thomas, J. O., and A. Y. Sader, J. Geophys. Res., 69, 4561 (1964).

32. Gringauz, K. I., Plan. and Space Sci., 11, 281 (1963).

33. Taylor, H. A., Jr., H. C. Brinton, and C. R. Smith, J. Geophys. Res., 70, 5769 (1965).

34. Serbu, G. P., and E. J. R. Maier, Goddard Space Flight Center Report X-615-66-92 (January 1966).

35. Scarf, F. L., R. W. Fredricks, and G. M. Crook, TRW Systems Report No. 99900-6019-R000 (August 1966).

36. Howard, H. T., V. R. Eshleman, G. H. Barry, and R. B. Fenwick, J. Geophys Res., 70, 4357 (1965).

37. Dessler, A. J., and F. C. Michel, J. Geophys. Res., 71, 1421 (1966).

38. Scarf, F. L., J. Geophys. Res., 71, 2709 (1966).

39. O'Brien, B. J., in Space Physics, ed. D. P. LeGalley and A. Rosen (J. Wiley and Sons, 1964), p. 505.

40. Van Allen, J. A., Radiation Trapped in the Earth's Magnetic Field, ed. B. M. McCormac (D. Reidel, 1966).

41. O'Brien, B. J., to appear in Proc. Inter-Union Symposium on Solar-Terrestrial Physics, Belgrade, 1966.

42. Frank, L. A., University of Iowa Technical Report 66-39 (August 1966).

43. Frank, L. A., University of Iowa Technical Report 66-48 (November 1966).

44. Davis, L. R., and J. M. Williamson, Space Research III, 365 (1963).

45. Wolfe, J. H., R. W. Silva, and M. A. Myers, Space Research VI (1966).

46. Taylor, H. E., and E. W. Hones, Jr., J. Geophys. Res., 70, 3605 (1965).

47. Kellogg, P. J., Nature 183, 1295 (1959).

48. Nakada, M. P., J. W. Dungey, and W. N. Hess, J. Geophys. Res., 70, 3529 (1965).

49. Parker, E. N., J. Geophys. Res., 65, 3117 (1960).

50. Davis, L., Jr., and D. B. Chang, J. Geophys. Res., 67, 2169 (1962).

51. Fälthammar, C. G., J. Geophys. Res., 70, 2503 (1965).

52. Nakada, M. P., and G. D. Mead, J. Geophys. Res., 70, 4777 (1965).

53. Frank, L. A., J. Geophys. Res., 70, 3533 (1965).

54. Dungey, J. W., Space Sci. Rev., 4, 199 (1965).

55. Fredricks, R. W., F. L. Scarf, and W. Bernstein, J. Geophys. Rev., 70, 21 (1965).

56. Dungey, J. W., Planet. and Space Sci., 11, 591 (1963).

57. Cornwall, J. M., J. Geophys. Res., 69, 1251 (1964).

58. Roberts, C. (see reference 40).

59. Hudson, H. S., G. K. Parks, D. W. Milton, and K. A. Anderson, J. Geophys. Res., 70, 4879 (1965).

60. Kennel, C. F., and H. E. Petschek, J. Geophys. Res., 71, 1 (1966).

61. Cornwall, J. M., J. Geophys. Res., 71, 2185 (1966).

62. Harris, E. G., J. Nucl. Energy, Pt. C, 2, 138 (1961).

63. Scarf, F. L., G. M. Crook, and R. W. Fredricks, J. Geophys. Res., 70, 3045 (1965); see also Radio Science, 1, 939 (1966).

64. Smith, R. L., J. Geophys. Res., 66, 3709 (1961).

65. Scarf, F. L., Phys. Fluids, 5, 6 (1962).

66. Liemohn, H. B., J. Geophys. Res., in press.

67. Smith, R. L., and N. M. Brice, J. Geophys. Res., 69, 5029 (1964).

68. Gurnett, D. A., S. D. Shawhan, N. M. Brice, and R. L. Smith, J. Geophys. Res., 70, 1665 (1965).

69. Gurnett, D. A., and N. M. Brice, J. Geophys. Res., 71, 3639 (1966).

70. Scarf, F. L., J. Geophys. Res., 67, 1751 (1962).

71. Sugiura, M., J. Geophys. Res., 66, 4087 (1959).

72. Judge, D. L., and P. J. Coleman, Jr., J. Geophys. Res., 67, 5071 (1962); Patel, V. L., Planet and Space Sci., 13, 485 (1965); Inouye, G. T., et al., TRW Systems Report 99900-6069-R000 (November 1966).

73. Parker, E. N., Phys. Fluids, 1, 171 (1958).

74. Scarf, F. L., J. H. Wolfe, and R. W. Silva, J. Geophys. Res., in press.

75. Brice, N. M., R. L. Smith, J. S. Belrose, and R. E. Barrington, Nature, 203, 926 (1964).

76. Iwai, A., J. Outsu, and Y. Tanaka, Proc. Res. Inst. Atmospheries, Nagoya Univ., 13, 1 (1966).

77. Perkins, F. W., E. E. Salpeter, and K. O. Yngvesson, Phys. Rev. Lett., 14, 579 (1965).

78. Rostoker, N., Nucl. Fusion, 1, 101 (1961).

79. Perkins, F. W., and E. E. Salpeter, Phys. Rev., 139, A55 (1965).

80. Tidman, D. A., Univ. of Maryland Tech. Note BN-426 (December 1965).

81. Chang, D. B. (see reference 40).

82. Coppi, B., G. Laval, and R. Pellat, Phys. Rev. Lett., 16, 1207 (1966).

83. Rosenbluth, M. N., and R. F. Post, Phys. Fluids, 8, 547 (1965).

84. Buneman, O., Phys. Rev. Lett., 10, 285 (1963).

85. Farley, D. T., Jr., Phys. Rev. Lett., 10, 279 (1963).

86. Chang, D. B., L. D. Pearlstein, and M. N. Rosenbluth, J. Geophys. Res., 70, 3085 (1965); 71, 351 (1966).

87. Swift, D. W., J. Geophys. Res., 70, 3061, (1965); also Univ. of Alaska Report NSF G-25193 (July 1965).

88. Scarf, F. L., W. Bernstein, and R. W. Fredricks, Trans. Amer. Geophys. Union, 47, 139 (1966).

89. Gurnett, D. A., Univ. of Iowa Report 66-27 (June 1966).

90. Mozer, F. S., and P. Bruston, J. Geophys. Res., 71, 4461 (1966).

91. Serlemitsos, P., J. Geophys. Res., 71, 61 (1966).

FIGURE CAPTIONS

Figure 1a. The idealized magnetosphere configuration in the noon-midnight meridian plane. The solar wind is incident from the left, the dashed lines represent the unperturbed dipole field, and the tail is not included.

1b. Solid lines: the Chapman-Ferraro current system which flows on the outside of the magnetosphere cavity and produces the distortion shown in 1a. Dashed lines: projection of current system which flows on magnetosphere surface and produces the cavity and the tail.

Figure 2. Schematic representation of the magnetosphere, the geomagnetic tail, and the "neutral" sheet. The distorted field lines are shown for the noon-midnight meridian plane, and the heavy dashed sections represent surface and return current systems.

Figure 3. Observations of the distorted geomagnetic field near the boundary. The curve labeled "theoretical" is the extrapolated dipole field. See text for further discussion.

Figure 4. Magnetic field measurements of the earth's magnetic tail by IMP-1 on orbit #41 inbound on May 2-4, 1964. The direction of the field closely parallels the earth-sun line with a rapid change in sense at a distance of 16 R_e. This is representative of the traversal of the magnetic neutral sheet in the earth's magnetic tail by IMP-1.

Figure 5. Possible neutral surface and tail field configuration for a large value of χ_{ss}, in the noon-midnight meridian plane. The corresponding orbit numbers and crossing positions from Figure 4 of Reference 16 are indicated. The hourly averaged vector measurements for $-1 < Y_{sm} < +1$ are superimposed.

Figure 6a. A meridian cross-section of the magnetosphere, showing three field-aligned whistler paths.

6b. Schematic spectrogram of typical whistlers caused by energy from a single lightning flash which propagates through the ducts A, B, and C and is received in the opposite hemisphere.

6c. The same as in (b), except that a knee is present between the paths B and C.

Figure 7. Spectrograms of knee whistlers recorded in the afternoon at Eights, Antarctica.

Figure 8. The magnetosphere under conditions of steady and moderate geomagnetic activity ($K_p \sim 2$-4). (a) Idealized meridian cross section typical of the early afternoon. The dashed portions of the "plasmapause" show the low altitude region in which the structure of the knee is not well known. (b) Idealized equatorial profiles typical of the afternoon and post-midnight hours.

Figure 9. Hydromagnetic Emission Band (characteristic fine structure consisting of a series of similar short wavetrains of increasing frequency).

Figure 10. Uncorrected response for the 1.7 kc/s channel of the TRW electric field detector on OV3-3 (the bandwidth depends on signal level, and the relevant adjustment has not been included), and amplitude of a 2 kc/s square wave voltage on the grid system of the Aerospace Corporation Faraday cup. When the grid just below the outer grounded grid is modulated (solid lines), the fringing fields apparently generate external plasma oscillations which are detected by the TRW antenna six feet away; these signals have no magnetic components. When a grid deep in the cup is similarly modulated (dashed lines), no external signals are generated and the observed electric fields are presumably ambient VLF oscillations.

Figure 11. Representative partial electron energy spectra obtained by L. A. Frank when OGO-3 was in the distant night-side magnetosphere.

Figure 12. Representative partial proton energy spectra obtained on OGO-3. The increase in flux near L = 3-4 may be associated with the knee, as discussed in the text.

Figure 13. Comparison of integral fluxes as measured by Davis and Williamson, and calculated integral fluxes. The calculated curves are normalized to the same peak flux for the lowest energy threshold. See Reference 52 for details.

Figure 14. Explorer 14 measurements of diffusion across L-shells.

Figure 15. The amplification ($A > 0$) or attenuation ($A < 0$) associated with the pressure anisotropy whistler mode instability. The parameters n, m refer to the loss cone distribution of Eq. (32).

Figure 16. An Injun 3 proton whistler sonogram, and a scaled drawing showing the local proton gyrofrequency (Ω_1) and the cross-over frequency ω_{12}. Here Ω_c represents the highest frequency for which polarization reversal occurs.

Figure 17. OGO-3 observations of multi-hump electron distributions in the distant magnetosphere.

Figure 18. The critical pressure gradients which give $\delta^2 W = 0$ for the distribution function of Eq. (45) are indicated by the shaded region, assuming κT_e is constant; any profile steeper than r^{-7} gives rise to an interchange instability. Since the whistler knee profile is considerably steeper than the critical one, the thermal energy must rise abruptly near the knee if the magnetosphere is to be flute stable.

Figure 19. A schematic diagram showing the interaction between the magnetospheric motions and the ionosphere. The electric field is such that $\vec{V} = C(\vec{E} \times \vec{B})/B^2$. The space charges occur where there is a shear in the plasma velocity field. Electron energization occurs in and under the region of negative space charge.

Figure 20. Representative latitudinal profiles of VLF hiss intensity and charged particle fluxes observed on Injun 3. The VLF hiss usually starts near the trapping boundary for 40 keV electrons, and the hiss is associated with the large flux of soft electrons having $E \sim 10$ keV.

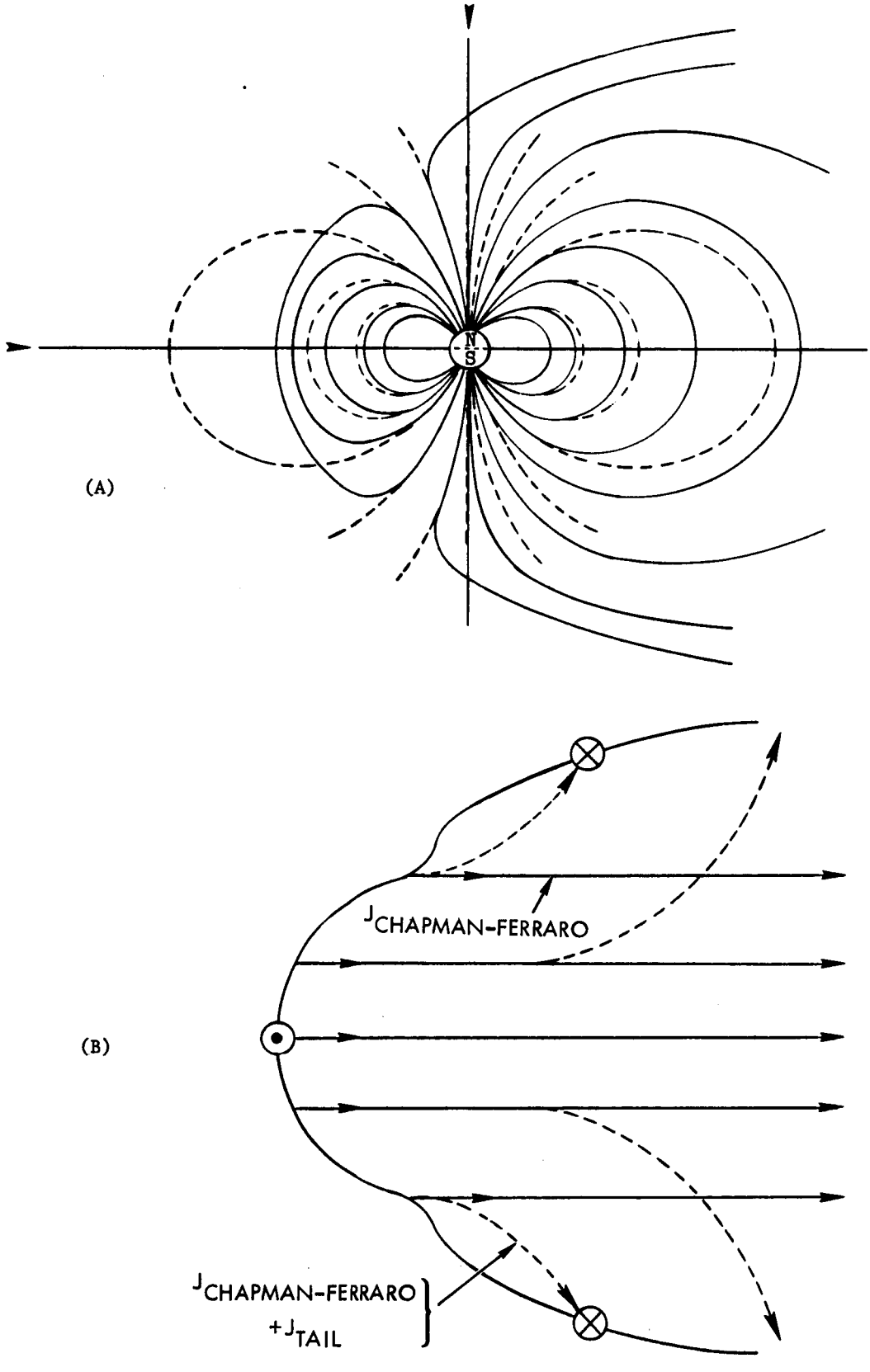

Figure 1

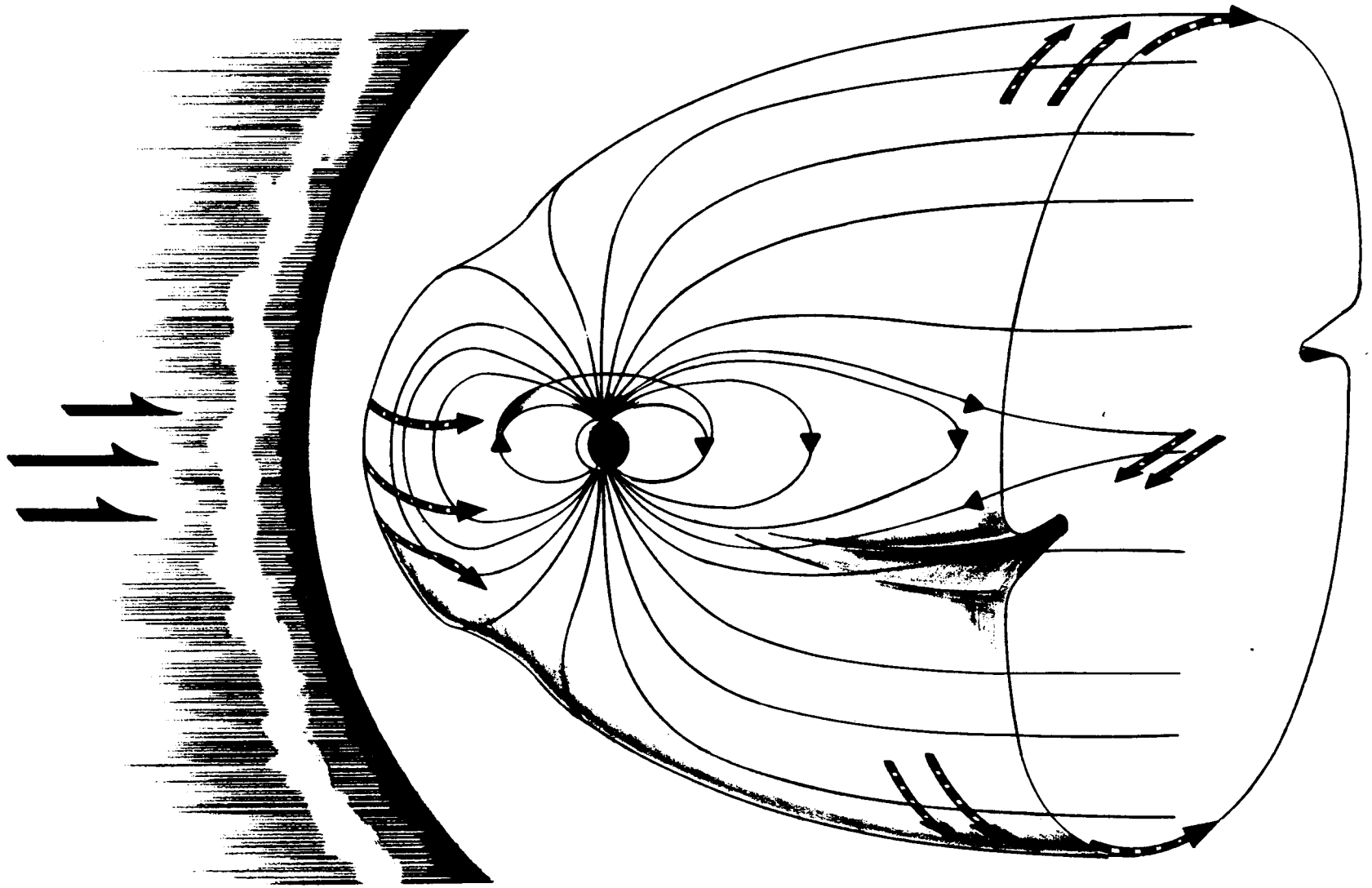

Figure 2

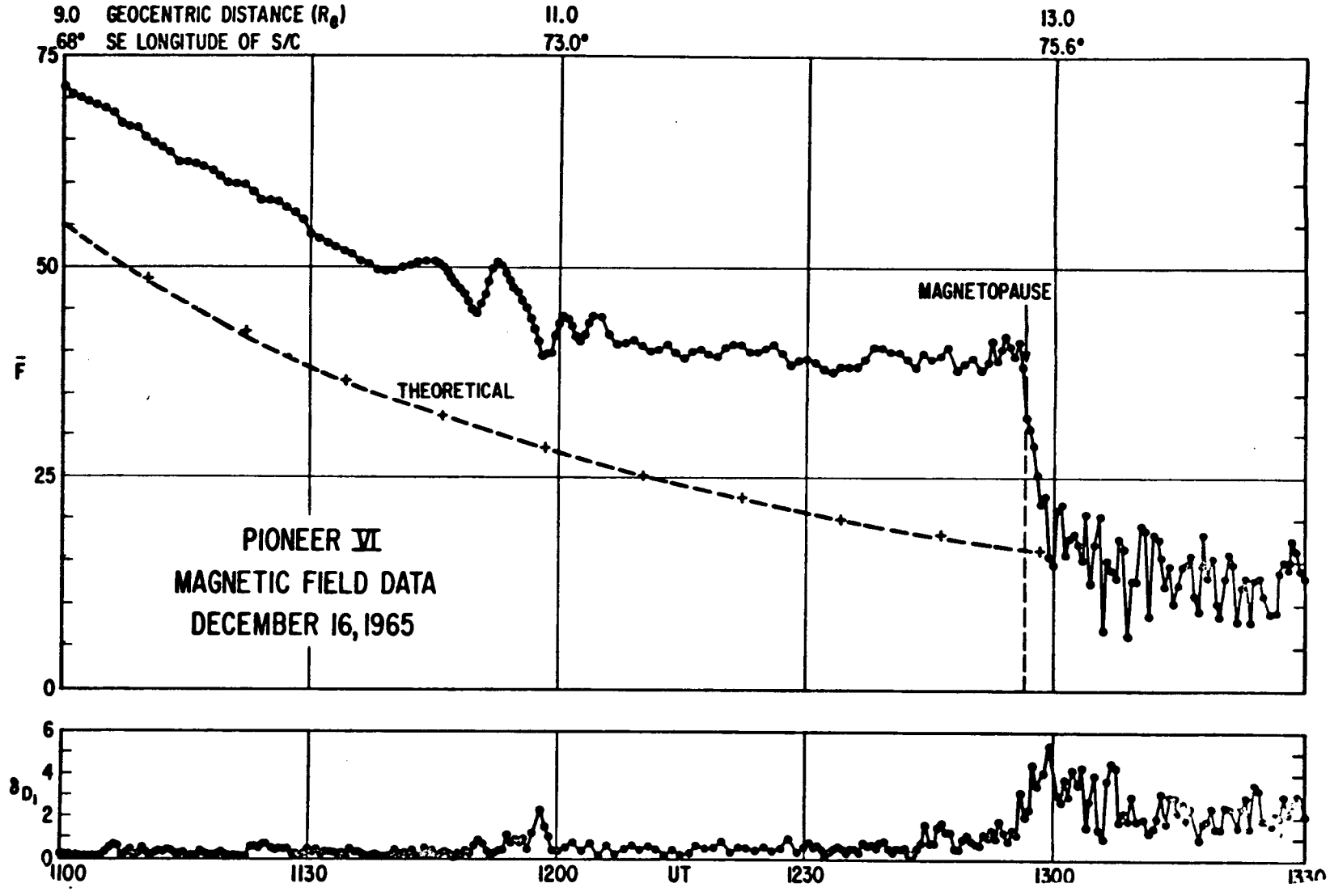
9.0 GEOCENTRIC DISTANCE (R_e)
68° SE LONGITUDE OF S/C
11.0
73.0°
13.0
75.6°
75
50
25
0
$\bar{F}$
MAGNETOPAUSE
THEORETICAL
PIONEER VI
MAGNETIC FIELD DATA
DECEMBER 16, 1965
6
4
2
0
δ_{D_1}
1100
1130
1200
UT
1230
1300
1330

Figure 3

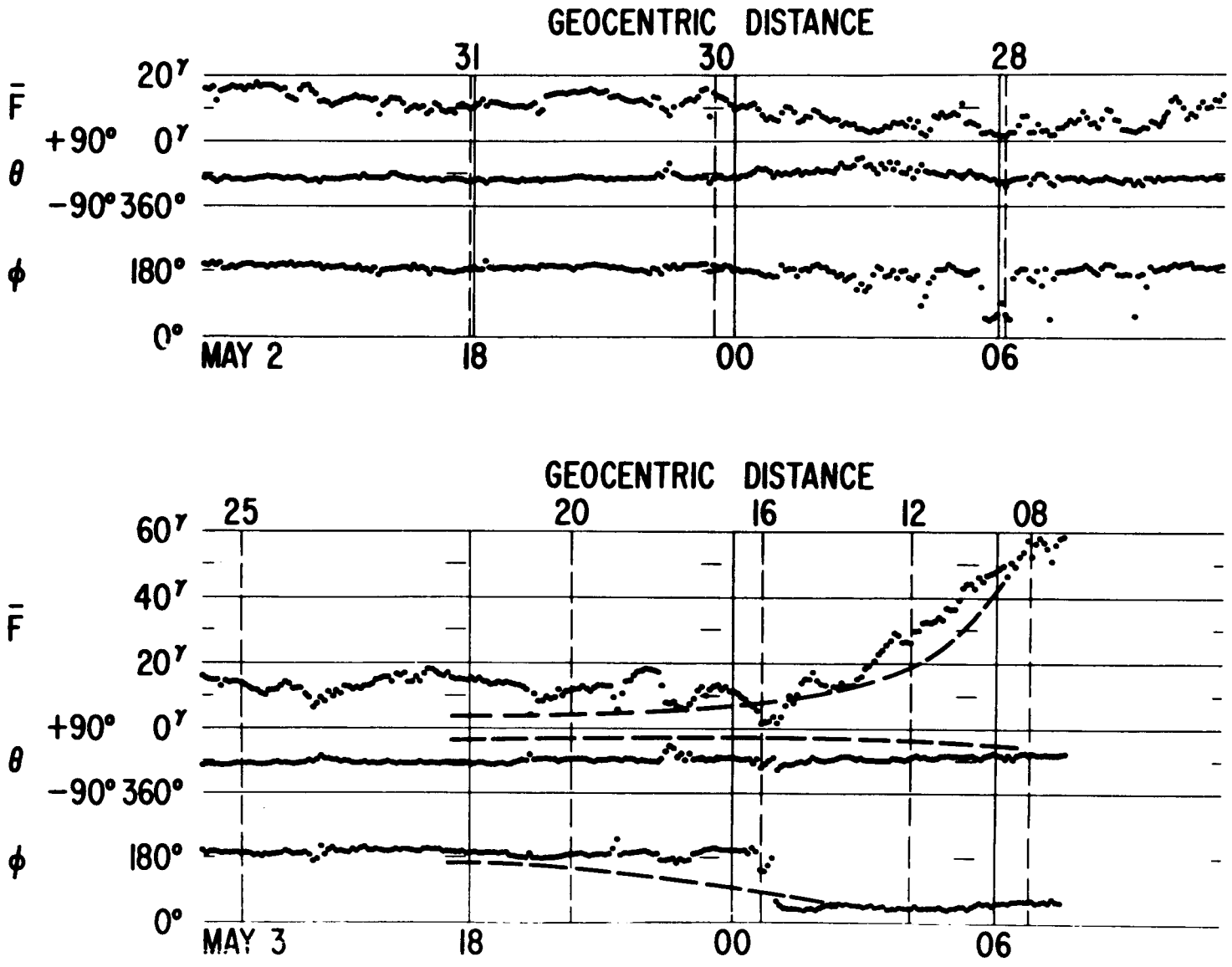
GEOCENTRIC DISTANCE
31
30
28
20γ
F̄
+90° 0γ
θ
-90° 360°
φ
180°
0°
MAY 2
18
00
06
GEOCENTRIC DISTANCE
25
20
16
12
08
60γ
40γ
F̄
20γ
+90° 0γ
θ
-90° 360°
φ
180°
0°
MAY 3
18
00
06

Figure 4

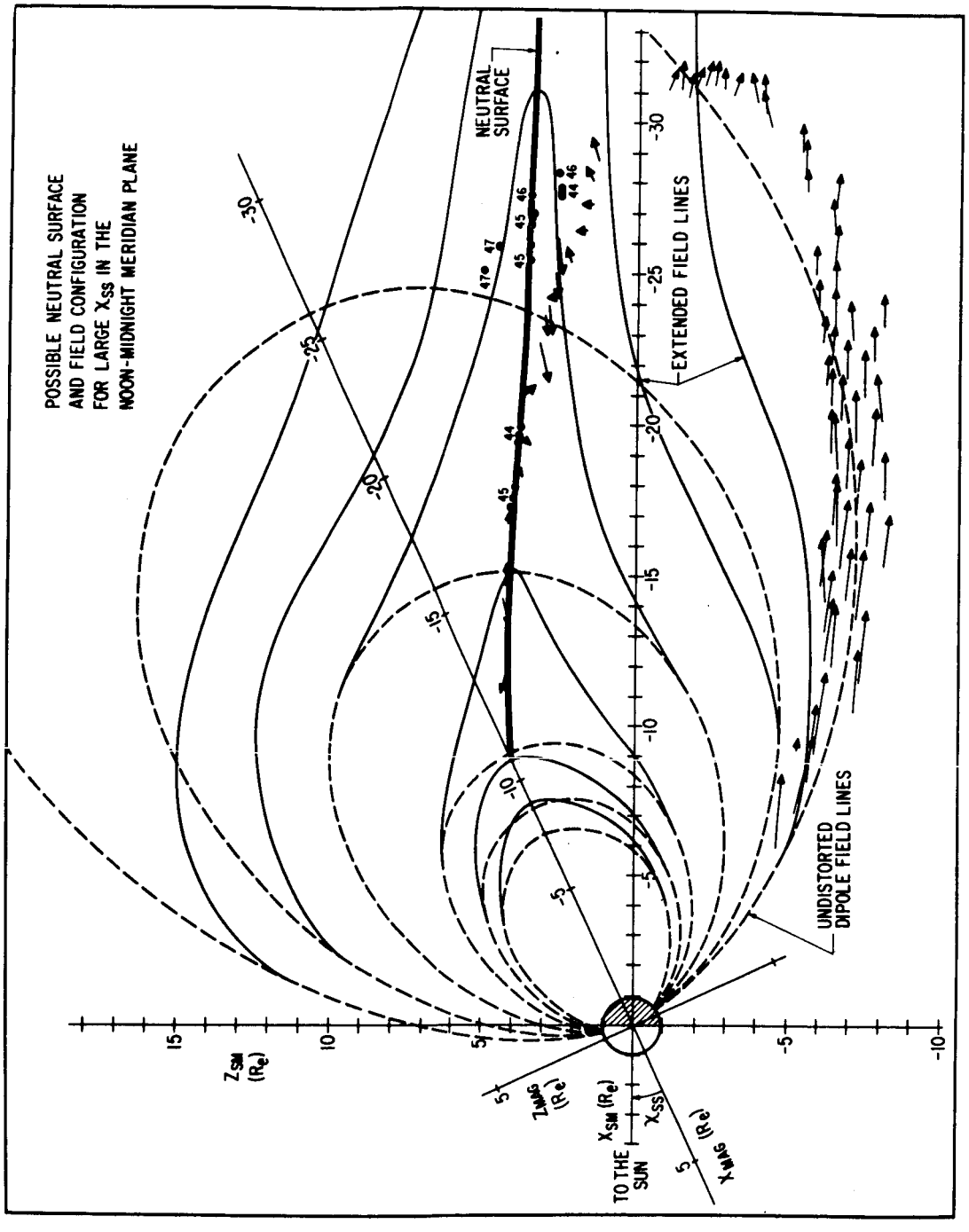
POSSIBLE NEUTRAL SURFACE
AND FIELD CONFIGURATION
FOR LARGE X_{SS} IN THE
NOON-MIDNIGHT MERIDIAN PLANE
NEUTRAL SURFACE
EXTENDED FIELD LINES
UNDISTORTED DIPOLE FIELD LINES
TO THE SUN
Z_{SM} (R_e)
Z_{MAG} (R_e)
X_{SM} (R_e)
X_{SS}
X_{MAG} (R_e)

Figure 5

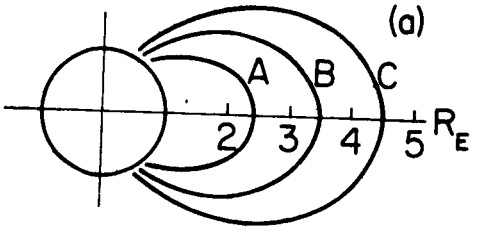
(a)
A
B
C
2
3
4
5
R_E

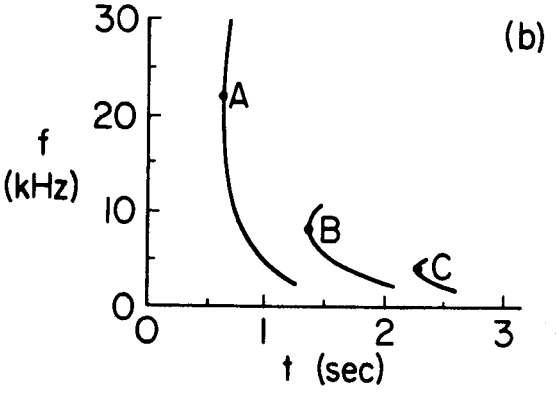
(b)
30
20
10
0
f
(kHz)
A
B
C
0
1
2
3
t (sec)

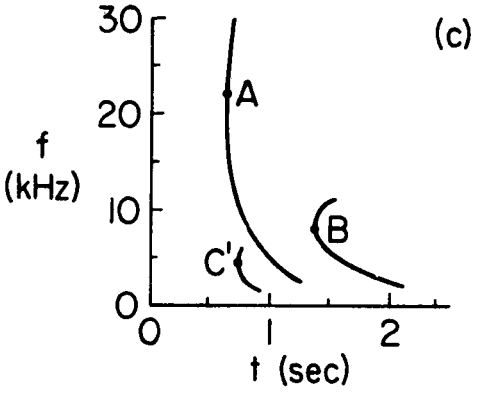
(c)
30
20
10
0
f
(kHz)
A
B
C'
0
1
2
t (sec)

Figure 6

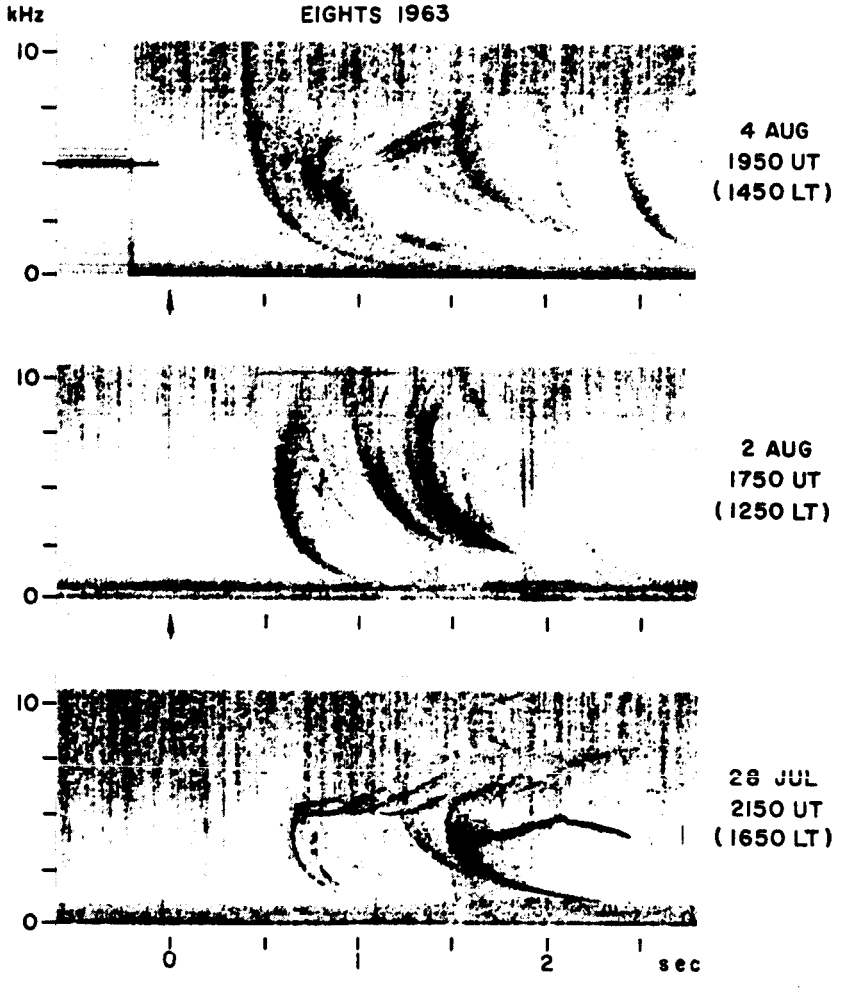
kHz
EIGHTS 1963
10
0
4 AUG
1950 UT
(1450 LT)
10
0
2 AUG
1750 UT
(1250 LT)
10
0
28 JUL
2150 UT
(1650 LT)
0
2
sec

Figure 7

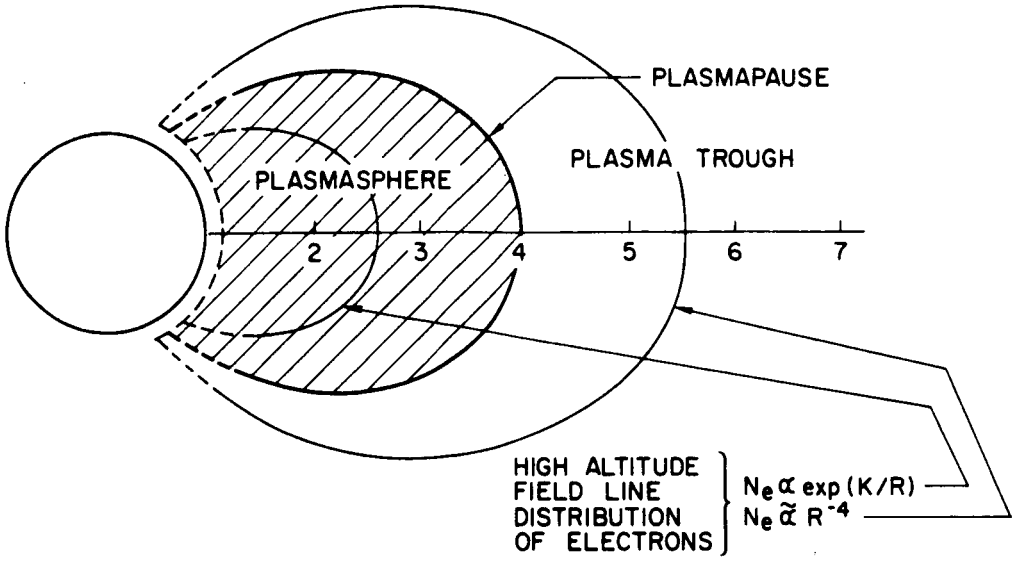
PLASMAPAUSE
PLASMA TROUGH
PLASMASPHERE
2
3
4
5
6
7
HIGH ALTITUDE FIELD LINE DISTRIBUTION OF ELECTRONS
$N_e \propto \exp(K/R)$
$N_e \propto R^{-4}$

(a)

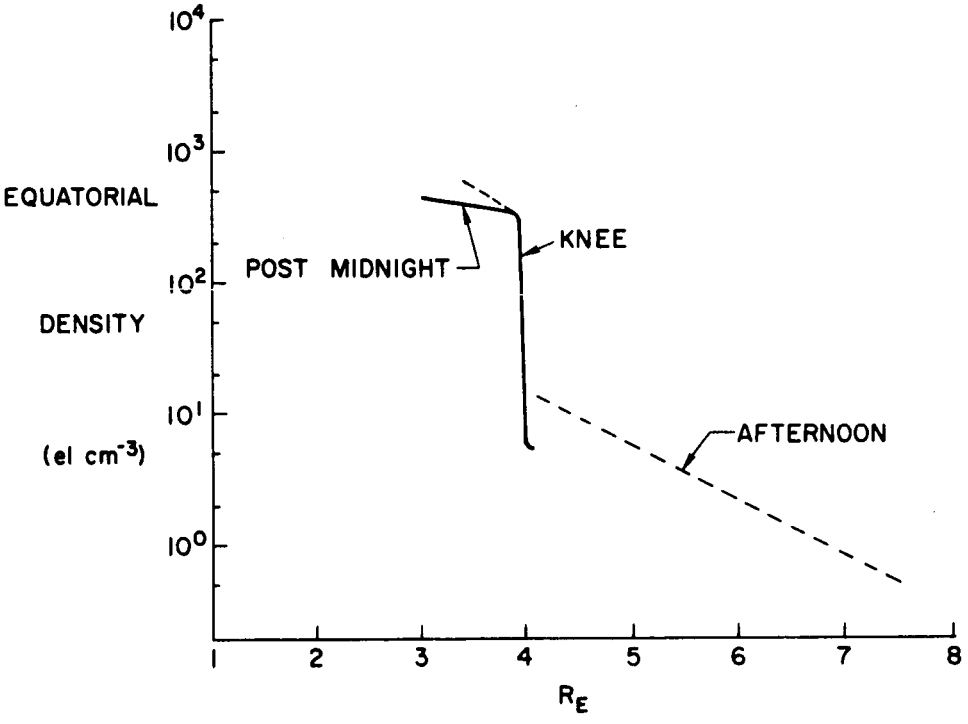
10^4
10^3
10^2
10^1
10^0
EQUATORIAL
DENSITY
(el cm^{-3})
POST MIDNIGHT
KNEE
AFTERNOON
1
2
3
4
5
6
7
8
R_E

(b)

Figure 8

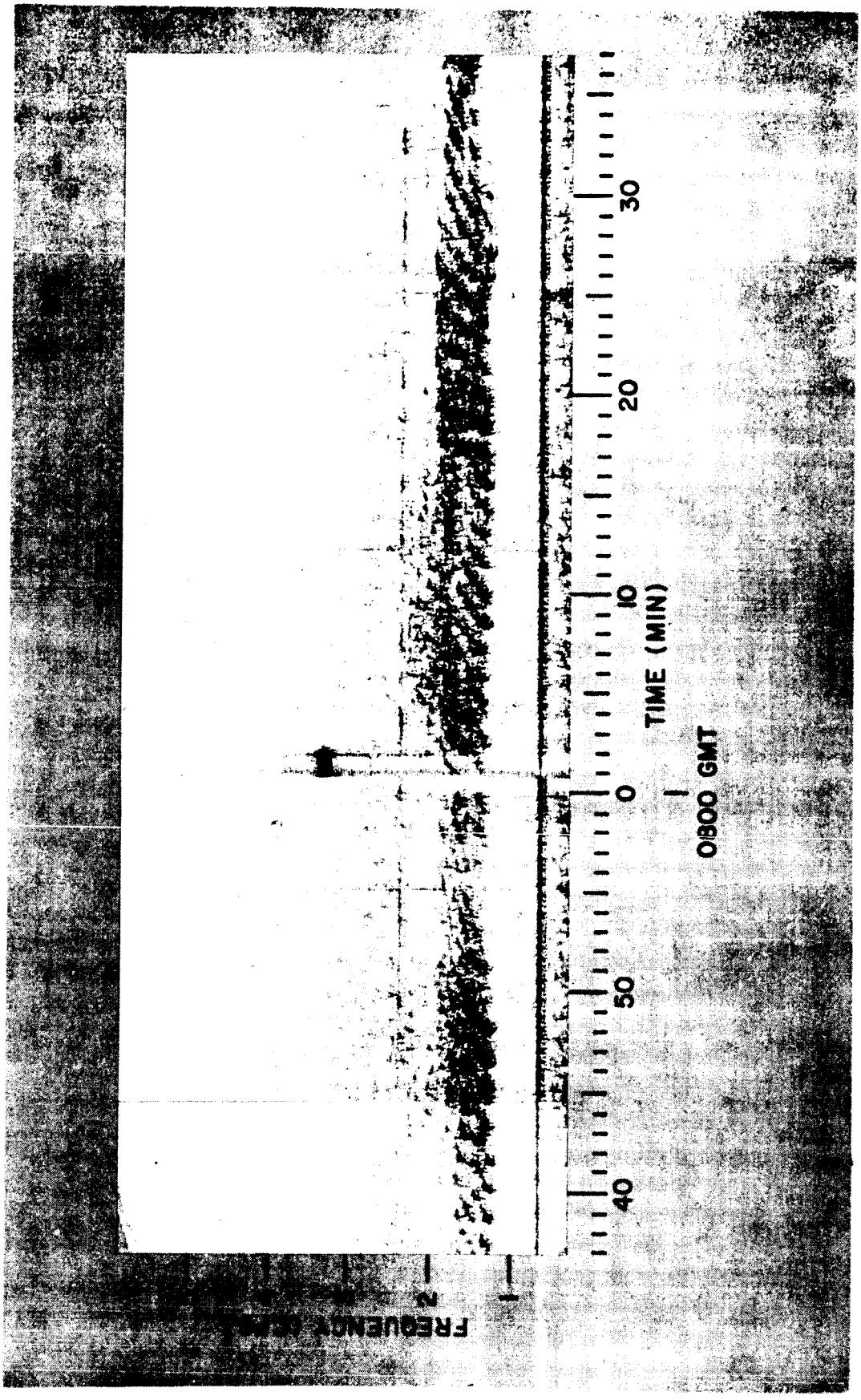

Figure 9

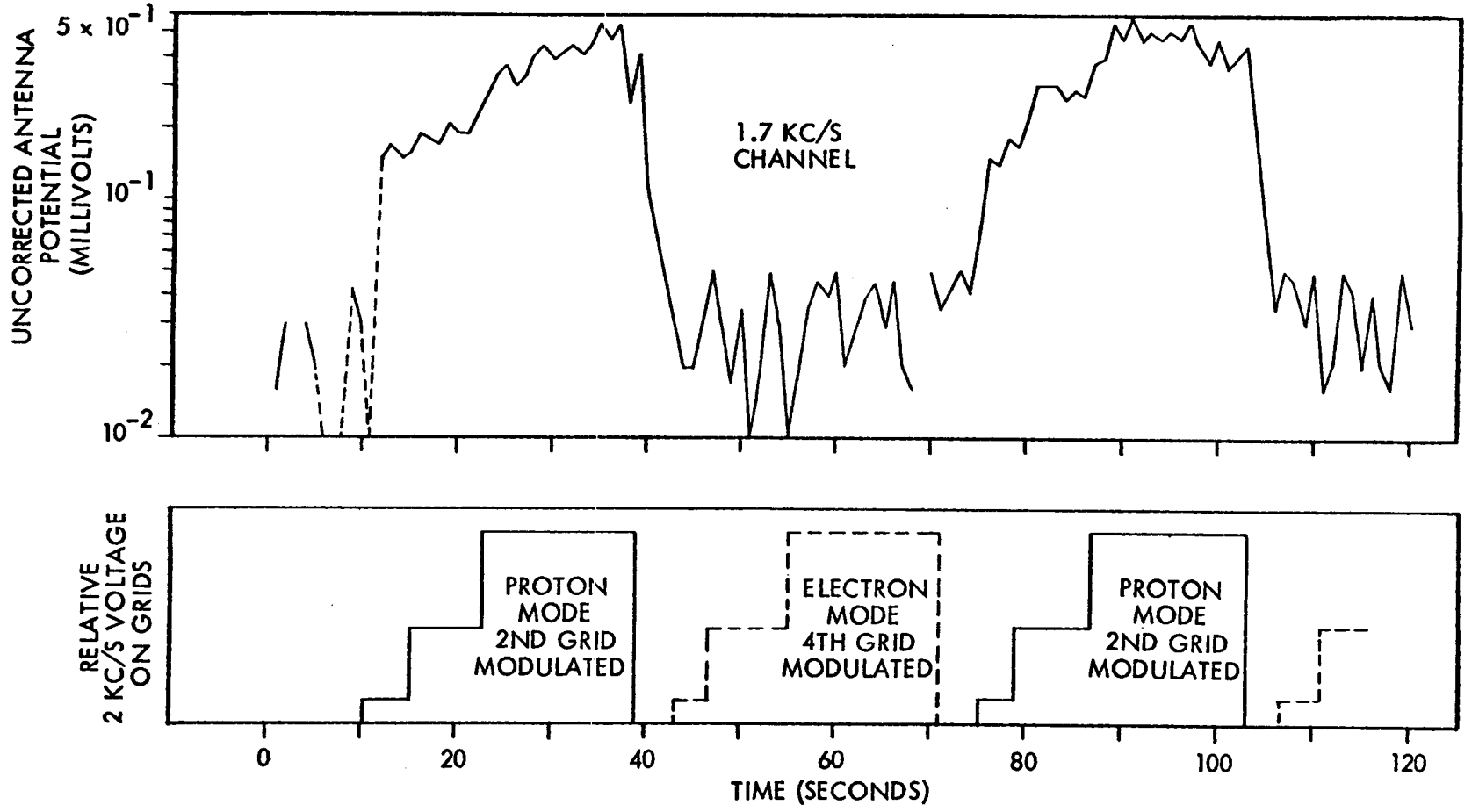
UNCORRECTED ANTENNA POTENTIAL (MILLIVOLTS)
5 x 10^-1
10^-1
10^-2
1.7 KC/S CHANNEL
RELATIVE 2 KC/S VOLTAGE ON GRIDS
PROTON MODE 2ND GRID MODULATED
ELECTRON MODE 4TH GRID MODULATED
PROTON MODE 2ND GRID MODULATED
0
20
40
60
80
100
120
TIME (SECONDS)

Figure 10

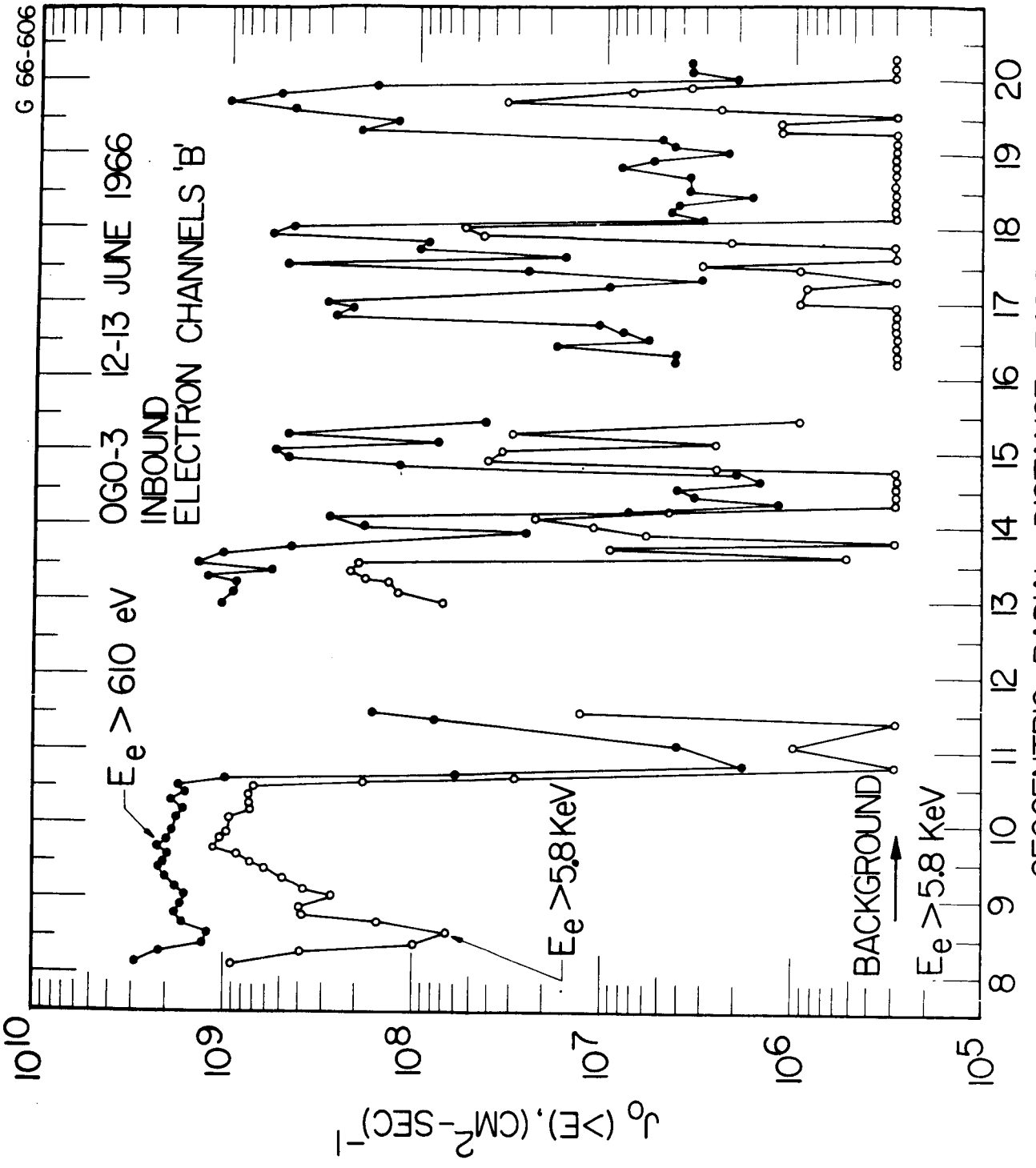
G 66-606
OGO-3 12-13 JUNE 1966
INBOUND
ELECTRON CHANNELS 'B'
E_e > 610 eV
E_e >5.8 KeV
BACKGROUND
E_e >5.8 KeV
J_o (>E), (CM^2-SEC)$^{-1}$
GEOCENTRIC RADIAL DISTANCE, EARTH RADII

Figure 11

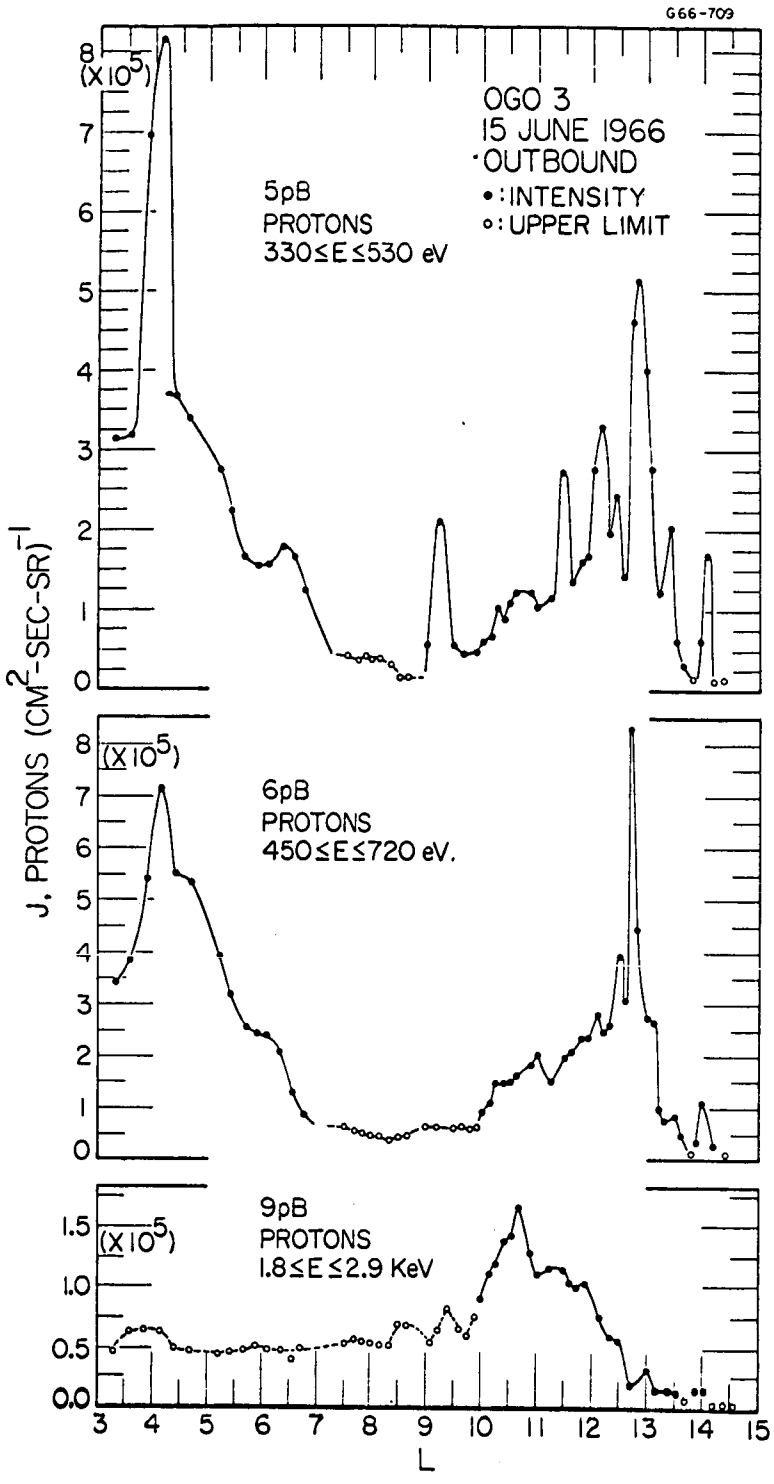
G66-709
OGO 3
15 JUNE 1966
OUTBOUND
•: INTENSITY
o: UPPER LIMIT
5pB
PROTONS
330≤E≤530 eV
6pB
PROTONS
450≤E≤720 eV.
9pB
PROTONS
1.8≤E≤2.9 KeV
(X10^5)
J, PROTONS (CM^2-SEC-SR)^-1
L

Figure 12

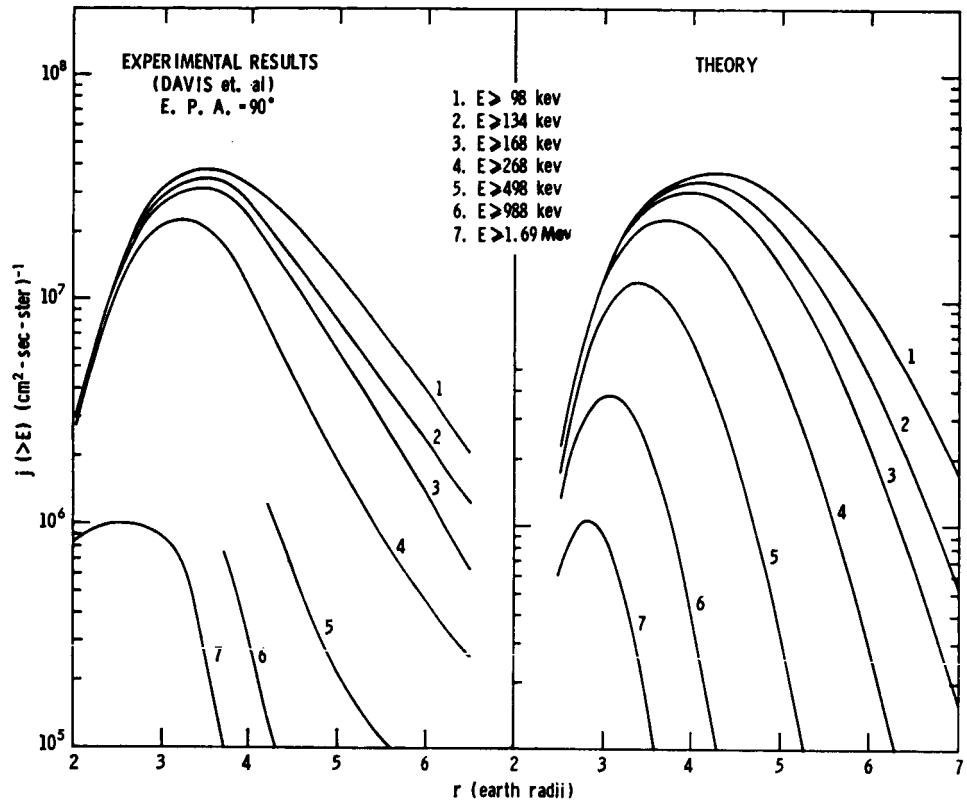
EXPERIMENTAL RESULTS
(DAVIS et. al)
E. P. A. -90°
THEORY
1. E> 98 kev
2. E>134 kev
3. E>168 kev
4. E>268 kev
5. E>498 kev
6. E>988 kev
7. E>1.69 Mev
j (>E) (cm²-sec-ster)⁻¹
r (earth radii)

Figure 13

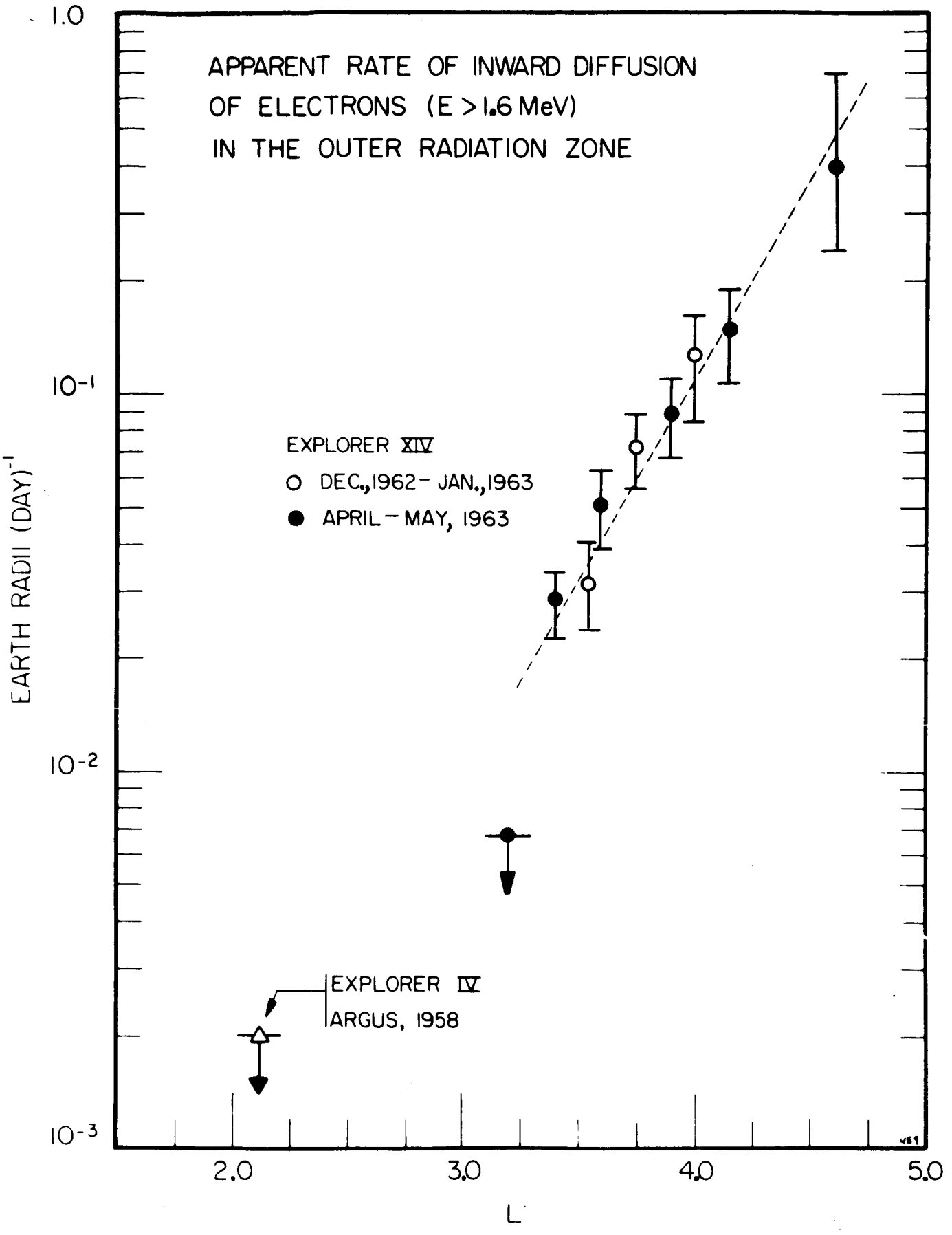
APPARENT RATE OF INWARD DIFFUSION
OF ELECTRONS (E > 1.6 MeV)
IN THE OUTER RADIATION ZONE
EXPLORER XIV
DEC., 1962 - JAN., 1963
APRIL - MAY, 1963
EXPLORER IV
ARGUS, 1958
EARTH RADII (DAY)$^{-1}$
1.0
10^{-1}
10^{-2}
10^{-3}
2.0
3.0
4.0
5.0
L

Figure 14

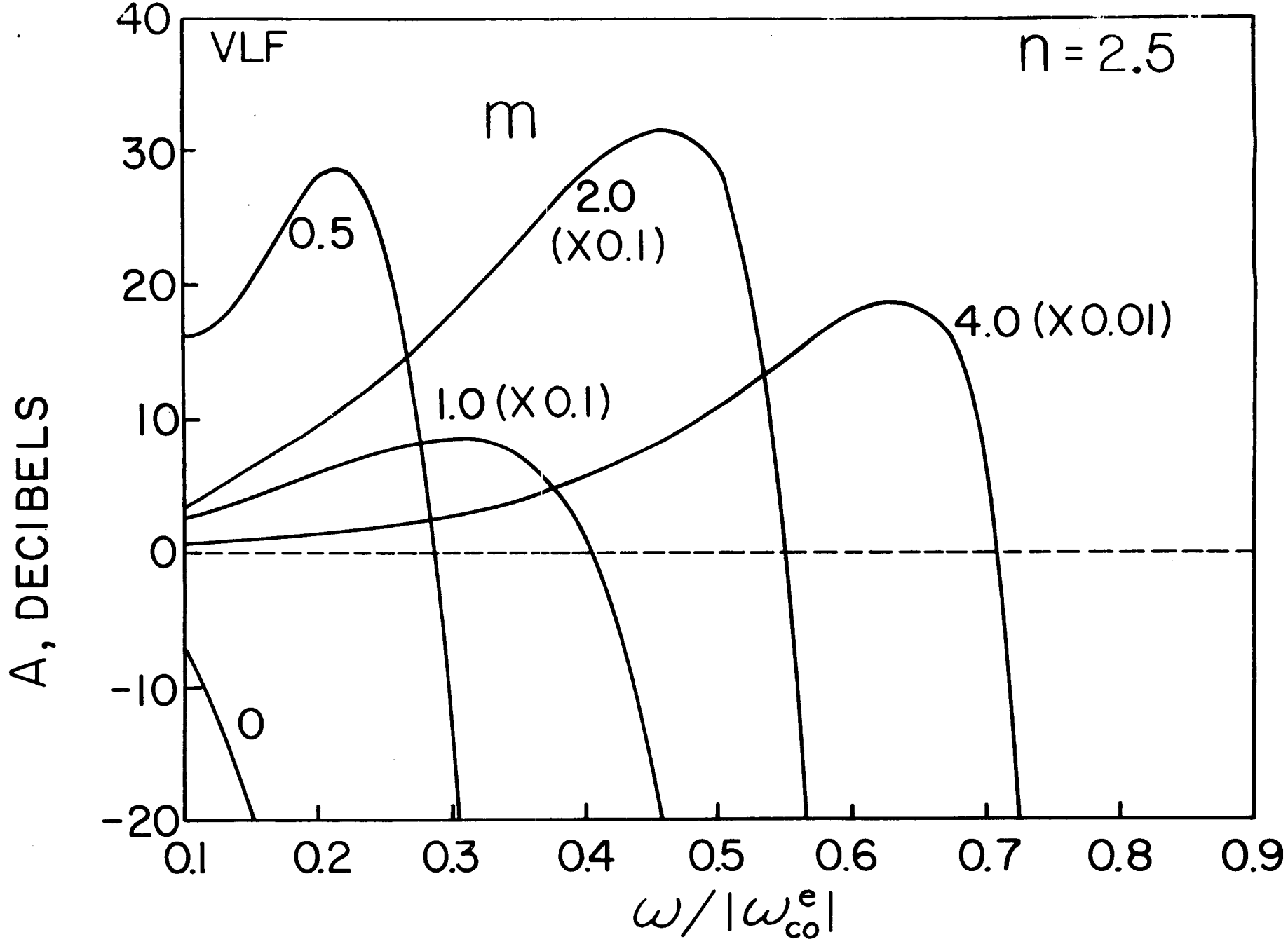
VLF
n = 2.5
m
0.5
2.0
(X0.1)
4.0 (X0.01)
1.0 (X0.1)
0
40
30
20
10
0
-10
-20
A, DECIBELS
0.1
0.2
0.3
0.4
0.5
0.6
0.7
0.8
0.9
ω/|ω^e_co|

Figure 15

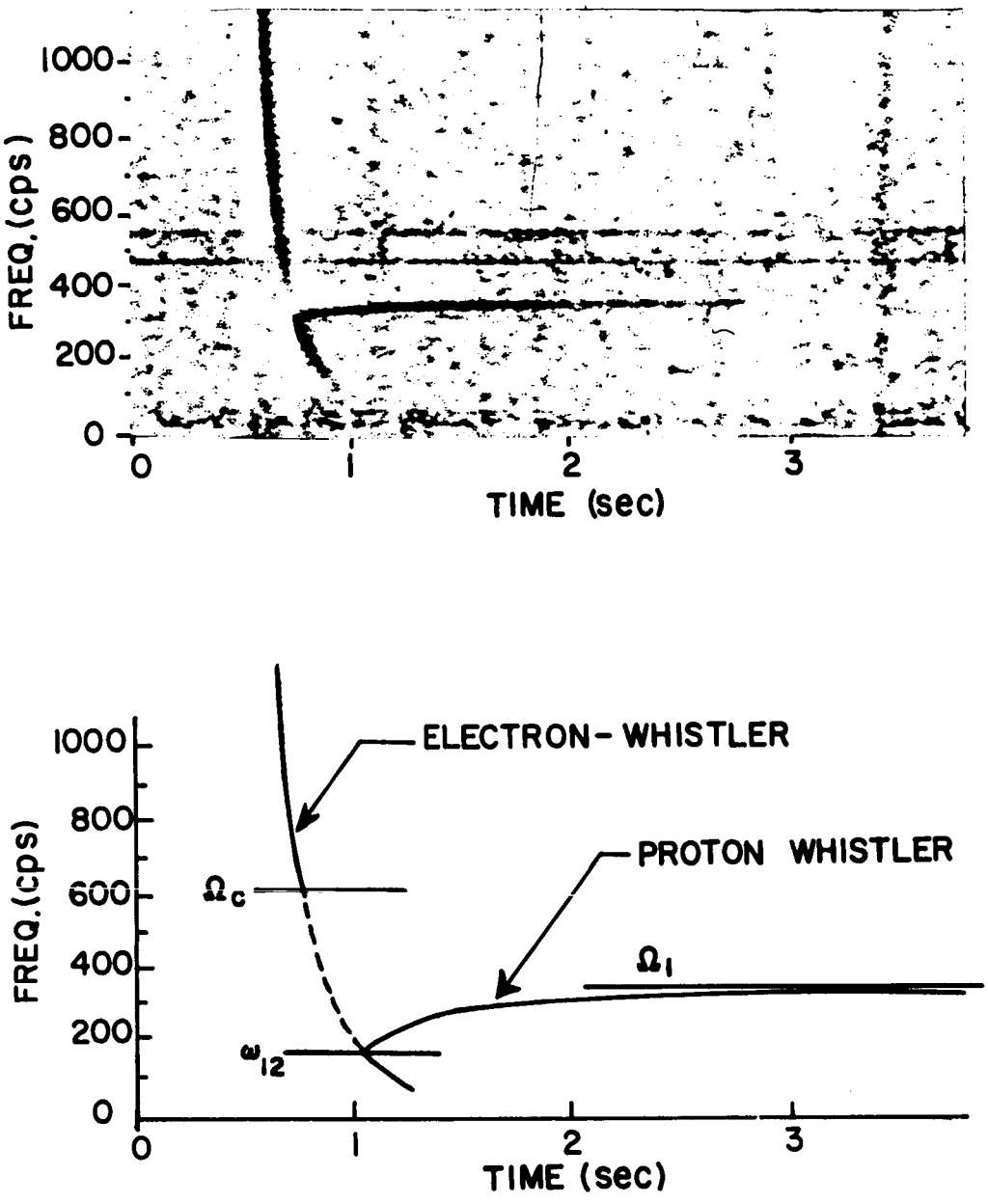

P-WHISTLER SPECTROGRAM AND NOMENCLATURE DIAGRAM

Figure 16

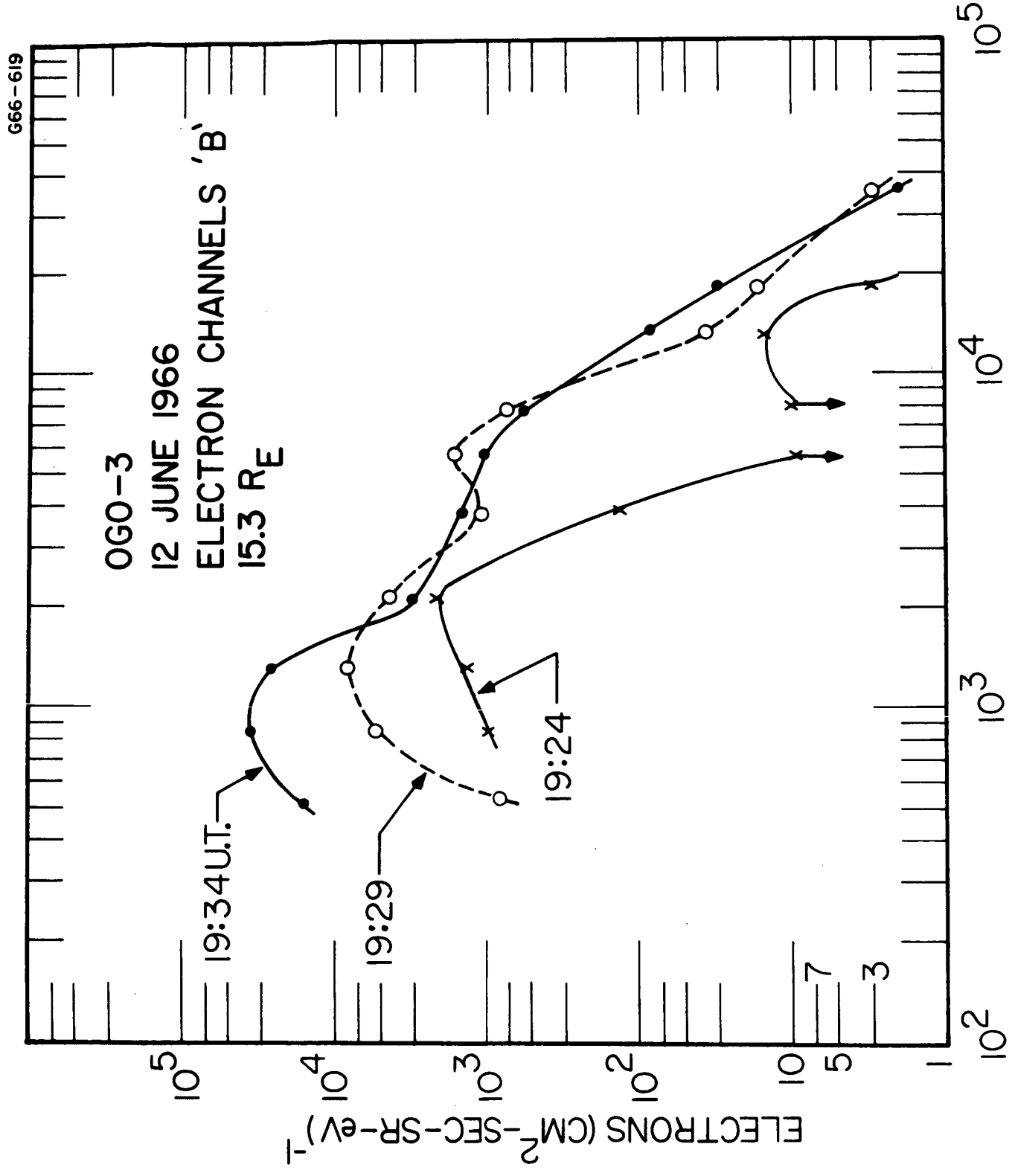
G66-619
OGO-3
12 JUNE 1966
ELECTRON CHANNELS 'B'
15.3 R_E
19:34 U.T.
19:29
19:24
ELECTRONS (CM^2-SEC-SR-eV)$^{-1}$
ELECTRON ENERGY, eV
10^5
10^4
10^3
10^2
10
7
5
3
1

Figure 17

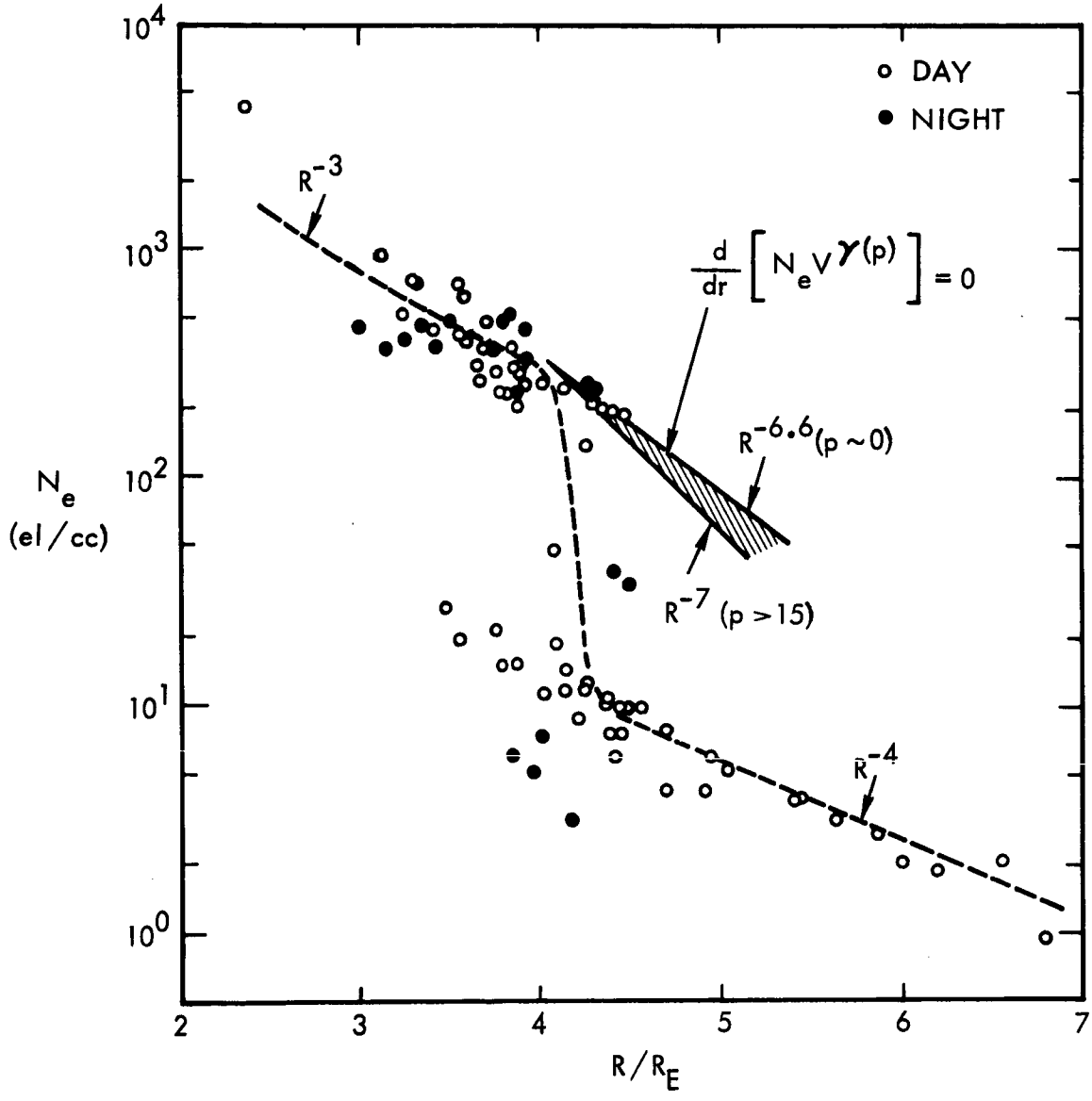
10^4
10^3
10^2
10^1
10^0
N_e
(el/cc)
o DAY
● NIGHT
R^{-3}
$\frac{d}{dr}\left[N_e V \gamma(p)\right] = 0$
$R^{-6.6}(p \sim 0)$
R^{-7} $(p > 15)$
R^{-4}
2
3
4
5
6
7
R/R_E

Figure 18

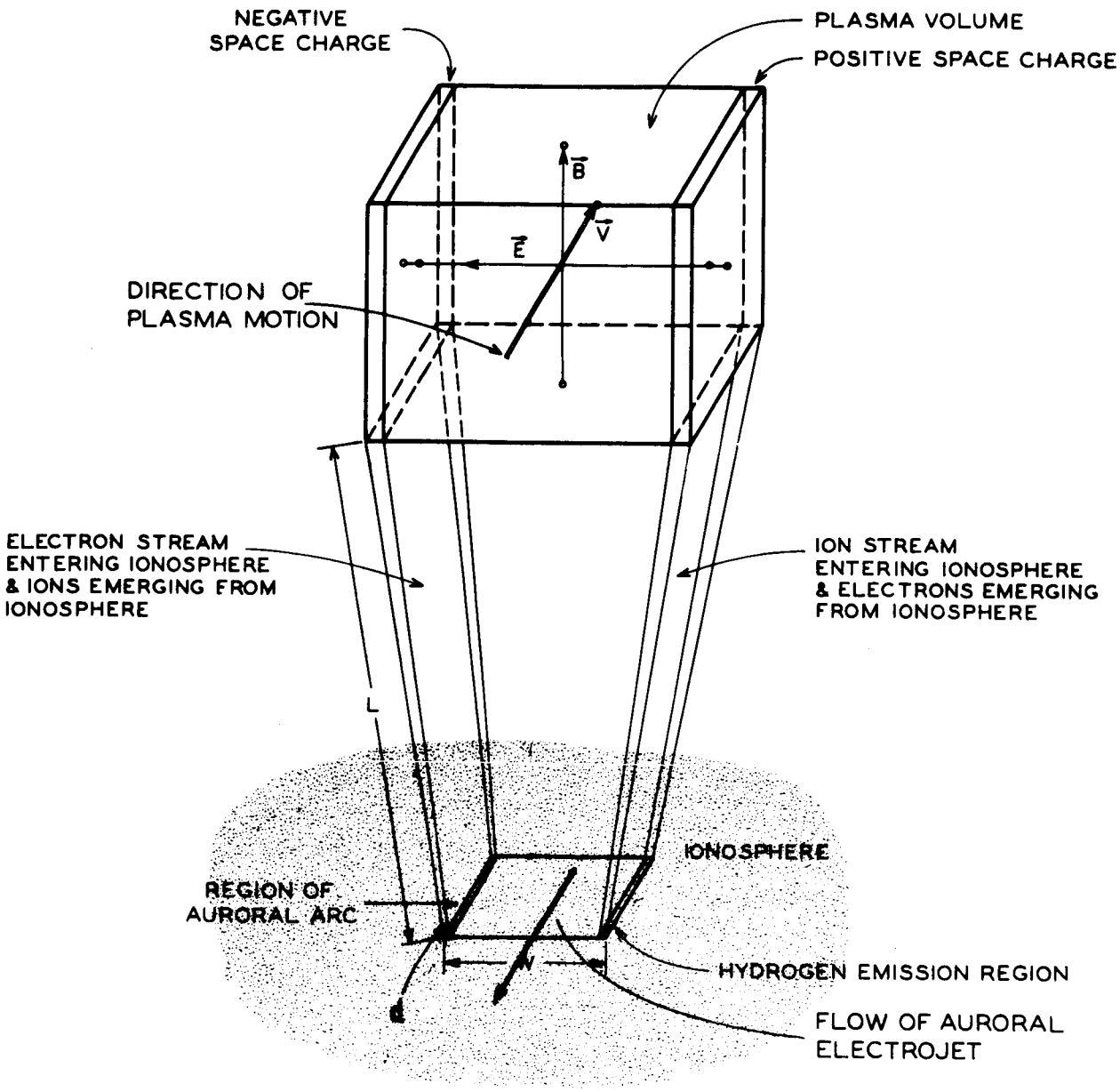
NEGATIVE
SPACE CHARGE
PLASMA VOLUME
POSITIVE SPACE CHARGE
B
E
V
DIRECTION OF
PLASMA MOTION
ELECTRON STREAM
ENTERING IONOSPHERE
& IONS EMERGING FROM
IONOSPHERE
ION STREAM
ENTERING IONOSPHERE
& ELECTRONS EMERGING
FROM IONOSPHERE
L
IONOSPHERE
REGION OF
AURORAL ARC
W
HYDROGEN EMISSION REGION
FLOW OF AURORAL
ELECTROJET

Figure 19

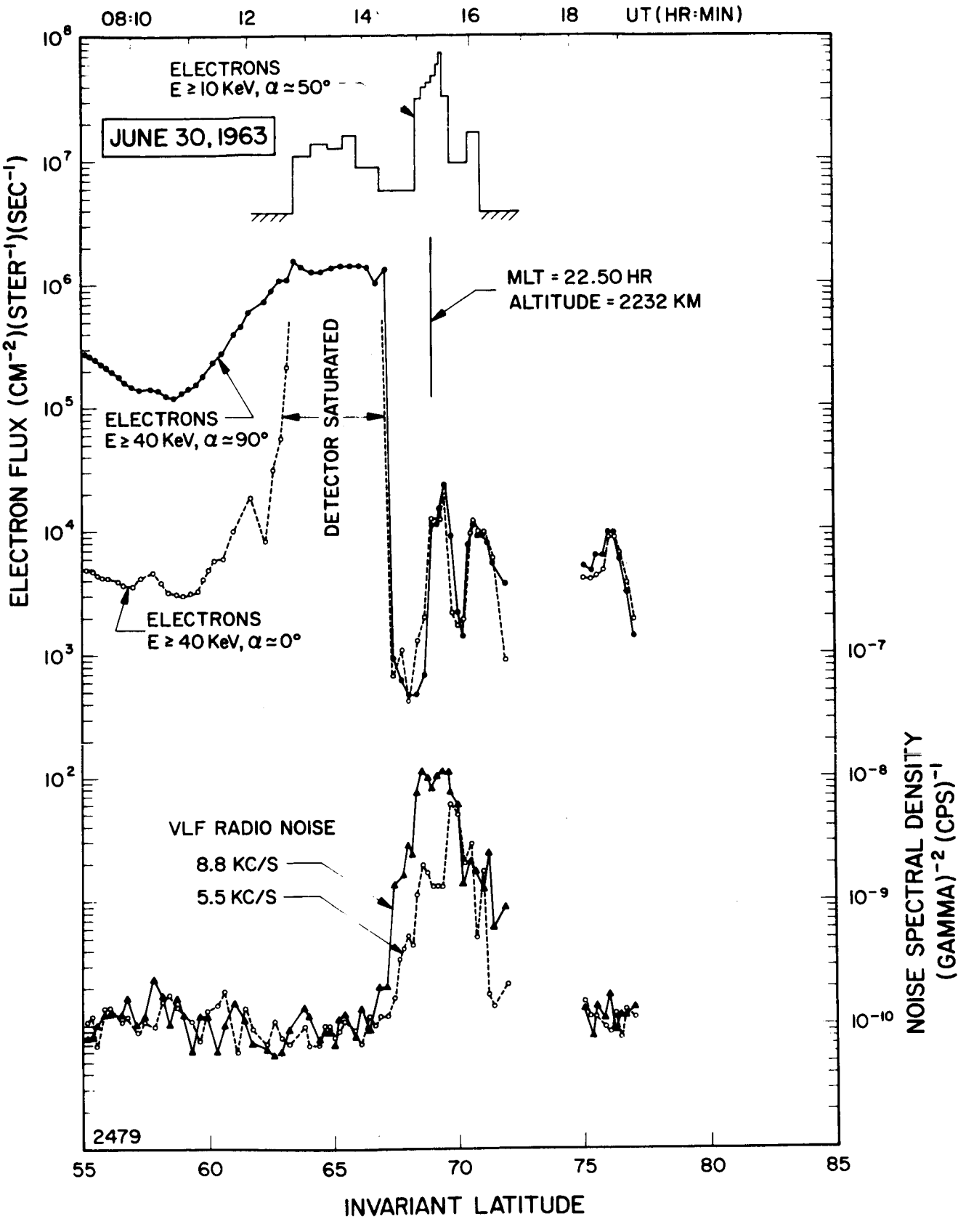
08:10
12
14
16
18
UT (HR:MIN)
ELECTRONS
E ≥ 10 KeV, α ≃ 50°
JUNE 30, 1963
MLT = 22.50 HR
ALTITUDE = 2232 KM
DETECTOR SATURATED
ELECTRONS
E ≥ 40 KeV, α ≃ 90°
ELECTRONS
E ≥ 40 KeV, α ≃ 0°
VLF RADIO NOISE
8.8 KC/S
5.5 KC/S
2479
ELECTRON FLUX (CM⁻²)(STER⁻¹)(SEC⁻¹)
NOISE SPECTRAL DENSITY (GAMMA)⁻² (CPS)⁻¹
INVARIANT LATITUDE
55
60
65
70
75
80
85

Figure 20